



INSTITUT DE FRANCE
Académie des sciences

Comptes Rendus

Mécanique


Breno Ribeiro Nogueira, Cédric Giry, Giuseppe Rastiello and Fabrice Gatuingt

One-dimensional study of boundary effects and damage diffusion for regularized damage models

Volume 350 (2022), p. 507-546

Published online: 1 December 2022

<https://doi.org/10.5802/crmeca.137>

 This article is licensed under the
CREATIVE COMMONS ATTRIBUTION 4.0 INTERNATIONAL LICENSE.
<http://creativecommons.org/licenses/by/4.0/>



Les Comptes Rendus. Mécanique sont membres du
Centre Mersenne pour l'édition scientifique ouverte
www.centre-mersenne.org
e-ISSN : 1873-7234



Short Paper / Note

One-dimensional study of boundary effects and damage diffusion for regularized damage models

Étude unidimensionnelle des effets de bords et de diffusion de l'endommagement pour des modèles d'endommagement régularisés

Breno Ribeiro Nogueira^{® a, b}, Cédric Giry^{® a}, Giuseppe Rastello^{® *, c}
and Fabrice Gatuingt^{® a}

^a Université Paris-Saclay, CentraleSupélec, ENS Paris-Saclay, CNRS,
LMPS - Laboratoire de Mécanique Paris-Saclay, 91190, Gif-sur-Yvette, France

^b DiBT, Engineering Division, University of Molise, via De Sanctis 1,
86100 Campobasso, Italy

^c Université Paris-Saclay, CEA Saclay, Service d'études mécaniques et thermiques,
91191 Gif-sur-Yvette Cedex, France

E-mails: breno.ribeiro_nogueira@ens-paris-saclay.fr (B. Ribeiro Nogueira),
cedric.giry@ens-paris-saclay.fr (C. Giry), giuseppe.rastello@cea.fr (G. Rastello),
fabrice.gatuingt@ens-paris-saclay.fr (F. Gatuingt)

Abstract. Local Continuum Damage Mechanics models cannot represent the entire degradation process in materials exhibiting strain-softening behaviors. It is well known that the rate equilibrium problem becomes ill-posed when softening occurs, and an infinity of solutions exists. From a numerical point of view, finite element analyses suffer from mesh-dependent results. Non-local models are generally used to regularize the structural response and recover objectivity. However, some physical inconsistencies can be observed in numerical results, e.g., damage diffusion over large damaged bands and damage attraction on the boundary of the computational domain. Non-local formulations with evolving interactions may better describe the damaging process and overcome these issues. This paper uses the so-called spalling test to underline the main drawbacks and advantages of several regularized models with constant and evolving non-local interactions. Concerning non-local formulations with constant interactions, attention is focused on the integral non-local formulation on the internal variable of the constitutive model and an implicit gradient damage formulation. Regarding formulations with evolving non-local interactions, attention is focused on a

* Corresponding author.

“stress-based integral non-local” approach and the so-called “eikonal non-local” approach. In this latter case, both its integral-type and gradient-type variants are considered.

Résumé. Les modèles d'endommagement classiques ne sont pas capables de représenter l'ensemble du processus de dégradation ayant lieu pendant l'adoucissement en déformation. Dans le cadre de la méthode des éléments finis, des résultats dépendants du maillage sont obtenus. Des modèles non-locaux sont généralement utilisés pour régulariser la réponse structurelle et retrouver l'objectivité vis-à-vis du maillage. Cependant, certaines incohérences physiques peuvent être observées, telles que la diffusion progressive de l'endommagement et son attraction par la frontière du domaine. Les approches non-locales avec interactions évolutives peuvent mieux décrire le processus de fissuration et surmonter ces problèmes. Dans cet article, le test d'écaillage est utilisé pour souligner certains inconvénients et avantages typiques de différentes méthodes de régularisation. En particulier, l'attention est portée sur la formulation intégrale non-locale sur la variable interne du modèle de comportement, sur une formulation à gradient implicite, sur une approche intégrale non-locale basée sur les contraintes et sur l'approche non-locale dite eikonale. Dans ce dernier cas, ses formulations intégrales et de type gradient sont considérées.

Keywords. Damage, Non-local regularization, Spalling test, Boundary effects, Damage diffusion.

Mots-clés. Endommagement, Régularisation non-locale, Écaillage, Bords, Diffusion de l'endommagement.

Manuscript received 25 March 2022, revised 11 July 2022 and 12 September 2022, accepted 15 September 2022.

1. Introduction

Strain-softening behaviors are observed in quasi-brittle materials such as concrete or some rocks. The stress–strain material response shows a progressive loss of stiffness right after the elastic limit. At the structural scale, the damage field tends to localize in a zone of vanishing volume. In a numerical context, this induces sensitivity to the spatial discretization of the considered structure, as Finite Element (FE) solvers do not converge upon mesh refinement. Moreover, this behavior can lead to spurious energy dissipation at the structural level, which is physically unacceptable [1].

This is not an inconvenience related to numerical approximations. From a mathematical viewpoint, the rate equilibrium problem becomes ill-posed [2], infinite linearly independent solutions can be obtained at the bifurcation point, and the size of the localization zone cannot be uniquely defined. In dynamics, the differential wave propagation equation is hyperbolic and becomes elliptic when localization occurs [3]. This implies that the structure is divided into two zones: one where elastic waves can propagate and another where the wave speed becomes imaginary. In [4], a mathematical analysis of localization is presented, which gives the specific conditions under which the strain localizes in narrow zones differently from the rest of the body. From a Continuum Damage Mechanics (CDM) viewpoint, the strain field becomes close to a Dirac distribution upon localization, which means that high strain gradients take place in small (but finite) zones. Consequently, the equivalent homogenized volume is not representative of what happens at lower scales. The assumption of distributed micro-cracks within the Representative Elementary Volume (REV) is no longer valid as the damage field is no more smooth [5].

One may employ some regularization techniques to guarantee a mesh-independent solution when dealing with strain softening numerically. One option is to apply a simple energetic regularization approach [6], defining material parameters on each element as a function of the dissipated fracture energy needed to create a crack surface for such a material. Nevertheless, several authors [7, 8] have shown that this regularization method implies different crack paths for different mesh orientations. Consequently, despite the regularization in terms of overall structural response, energy-based methods are not recommended for dealing with more sophisticated analyses, which are expected to give information about crack paths and failure modes.

A more physical way to regularize the structural response is to introduce a characteristic/internal length l_c (intrinsically related to a characteristic time in dynamics) to describe the spatial interactions at a lower scale and define a range of validity of the theory considered for

the analysis. In continuum mechanics, a l_c related to the size of the REV and the Fracture Process Zone (FPZ) [9, 10] may be introduced into the constitutive relations. In quasi-static analyses, this is usually done by using the so-called non-local damage theory [1], averaging a specific variable through a convolution product with a given weight function. Since then, various non-local approaches have been developed, and the subject is a large field of research.

The introduction of some micro-structural information into the macroscopic models can also be represented by many other approaches. Gradient approaches, for instance, were firstly introduced in plasticity [11–14], where higher-order gradients of the equivalent plastic strain are used in the constitutive relations. Influenced by these ideas, gradient-enhanced formulations were also introduced in damage mechanics [15, 16] taking into account the influence of the spatial interaction between points on damage growth. Other methods have also been used for regularizing damage problems such as the delay damage models (e.g., [17–19]), the Thick Level Set (TLS) approach [20], the phase field approach [21, 22], and more recently the Lip-field approach [23].

The present work analyzes and compares numerically several non-local damage formulations, particularly regarding the obtained damage evolution close to the domain's boundaries and/or in highly damaged zones. Following previous works in literature, numerical studies are performed by simulating the so-called spalling phenomenon, i.e., the tensile failure under an impact compression load. Experimentally, this loading condition is obtained thanks to Hopkinson-bar spall experiments [24–26]. It is well known that local damage models cannot reproduce the experimental spalling, as strain localization will inevitably lead to an ill-posed boundary value problem and, therefore, mesh-dependent results. Classical non-local models (i.e., with a constant characteristic length) should naturally recover objectivity but fail to determine the spalling thickness. For instance, damage attraction on the boundary has been reported [27], leading to non-physical spalling failures. Simone *et al.* [28] showed that classical integral or implicit gradient theories fail to describe damage initiation, especially near strong strain field variations, which were not related to boundary effects. In addition, the damage profile is spread on a finite zone instead of a localized one, as expected.

Bažant [29] studied the interaction between micro-cracks and showed that if damage is not sufficiently small, the weight function should depend on the stress state in the vicinity of a given point. In other words, the non-local interactions need to evolve while damage grows, instead of remaining isotropic and constant throughout the fracture process. Geers *et al.* [30] showed that the classical implicit gradient damage model fails when treating highly damaged zones. Thus, they proposed a strain-based transient-gradient damage model, considering that the gradient parameter c (proportional to l_c) evolves in function of the local strain state. Giry *et al.* [31] proposed a stress-based non-local damage model, which lets the internal (or characteristic) length evolve as a function of the stress state. The evolution of non-local interactions was also proposed in many other damage models based on the stress, strain, damage or the microstructure (e.g., [32–40]).

This paper focuses on five non-local approaches for regularizing the damage problem. Localization is studied considering a one-dimensional (1D) dynamic problem. The latter is not intended to reproduce the dynamic material behavior but is used here as a localization tool. An explicit dynamic 1D FE analysis code is therefore developed to illustrate the advantages and drawbacks of each approach.

2. Non-local damage formulations

In the present work, CDM [41] is used to describe material degradation. In the following, all the formulations are written for the 1D case for conciseness. Similar formulations can be introduced for modeling multi-dimensional problems.

2.1. Local model

In the isotropic case, one may consider a scalar damage variable D evolving from zero (virgin material) to one (fully damaged material). Following a thermodynamic framework, the Helmholtz free energy potential and the intrinsic dissipation read $\rho\psi = \rho\psi(\epsilon, D) = 1/2(1 - D)E\epsilon^2$ and $\mathcal{D} = Y\dot{D}$, respectively. Here, E is the Young modulus, ϵ is the small strain, and $Y = -\rho\partial\psi/\partial D$ is the energy release rate. The Cauchy stress is thus written as:

$$\sigma = \rho \frac{\partial\psi}{\partial\epsilon} = (1 - D)E\epsilon. \quad (1)$$

Damage is considered to evolve according to the exponential law [42]:

$$D = g(\kappa) = 1 - \frac{\kappa_0}{\kappa} \exp(-B(\kappa - \kappa_0)), \quad (2)$$

where:

$$\kappa = \max_t(\kappa_0, e) \quad (3)$$

is a damage-driving history variable taking into account the maximum value reached by an equivalent strain measure (e) throughout the loading history (κ_0 denotes the damage activation threshold), and B is the damage brittleness. In this study, the equivalent strain is defined as the positive part of the strain (i.e., if $\epsilon > 0$, $e = \epsilon$; else $e = 0$).

2.2. Regularization methods

FE analyses of softening media suffer from mesh-dependent results. Local damage models inevitably induce spurious energy dissipation, given that damage localizes in a zone of vanishing volume upon mesh refinement. To counteract this problem, regularization methods have been proposed in the literature, taking into account additional quantities to describe the localization process.

In non-local models, the constitutive relation is a function of what occurs in the entire body. Neighborhood (non-local) interactions are therefore used to enrich the continuum description by adding higher-order gradients or spatial averaging. Two main families of non-local models are considered in this work:

- (i) **Integral formulations.** Pijaudier-Cabot and Bažant [1] proposed a non-local integral damage theory, where the local field related to the damage evolution is replaced by its weighted average over the whole volume of a body Ω . A common choice in FE calculations is to average the variable that drives damage evolution (the strain in this example).¹ In this case, one has:

$$\bar{e}(x) = \frac{1}{V_r(x)} \int_{\Omega} \phi(l_{xy}, l_c) e(y) dy \quad V_r(x) = \int_{\Omega} \phi(l_{xy}, l_c) dy, \quad (4)$$

where $l_{xy} = |x - y|$ is the Euclidean distance between points x and y in Ω , and $\phi(l_{xy}, l_c)$ is a weight function generally taken as a Gaussian distribution,² i.e.:

$$\phi(l_{xy}, l_c) = \exp\left(-4 \left(\frac{l_{xy}}{l_c}\right)^2\right). \quad (5)$$

¹Jirásek [43] tested different ways of introducing non-locality in damage formulations. Notably, he showed that averaging D would lead to stress locking behaviors, which could not describe the crack initiation. In a 1D context, he showed that formulations that average either Y or ϵ are more capable of describing the degradation process. Moreover, damage formulations which average the strain are more suitable for FE calculations considering nonlinear behaviors depending on the strain state.

²Another possibility is to use a bell-shaped function, which has a bounded support, instead of an unbounded one as in the case of the Gaussian function.

The normalizing factor $V_r(x)$ figuring in (4) guarantees that a uniform field is not modified by the convolution product, which, however, induces spurious behavior close to the boundary, as we will see later on.

- (ii) **Gradient formulations.** Peerlings *et al.* [16] proposed a gradient-enhanced damage formulation which is obtained from the conventional integral non-local theory, substituting the local equivalent strain in (4) by its Taylor expansion. A more numerical-friendly approach is obtained by differentiating two times the resulting explicit equation and neglecting higher-order terms [5]. The non-local equivalent strain is now the solution of the following Helmholtz-like differential equation:³

$$\bar{e}(x) - c \frac{d^2 \bar{e}(x)}{dx^2} = e(x) \quad \text{in } \Omega \quad \text{with} \quad \frac{d\bar{e}(x)}{dx} = 0 \quad \text{on } \partial\Omega, \quad (6)$$

with c being a model parameter (homogeneous to the square of a length) and $\partial\Omega$ denoting the boundary of Ω . This formulation is referred to as the “implicit gradient damage approach” and represents a strong form of non-locality, as long-range interaction between points is allowed. To provide the variational formulation corresponding to (6), let us introduce the non-local virtual strains admissibility set:

$$\mathcal{E} = \{\eta \mid \eta(x) \in H^1(\Omega)\}. \quad (7)$$

The problem to be solved for computing the non-local equivalent strain field thus reads:

$$\int_0^L c \frac{d\bar{e}}{dx} \frac{d\eta}{dx} dx + \int_0^L \bar{e}\eta dx = \int_0^L e\eta dx \quad \forall \eta \in \mathcal{E}, \quad (8)$$

where the natural boundary condition has been used [12, 14, 16]. In the previous equation the dependency of (e, \bar{e}, η) on the space variable x was omitted for the sake of conciseness.

A comparison of integral non-local and explicit/implicit gradient models can be found in [44], where it is shown that the explicit gradient formulation allows only interaction between points at infinitesimal distances. Therefore, this formulation and other higher-order gradient ones are classified as weakly non-local models [10] and can be seen even as local from a mathematical viewpoint [44]. In the following, the classical integral non-local formulation and the corresponding implicit gradient-enhanced formulation will be named INL and GNL, respectively.

2.3. Non-local models with evolving internal length

Several authors proposed to take into account the influence of the damaging process on non-local interactions. In general, one aims to completely simulate the strain localization process from diffused damage (i.e., micro-cracking phase) to damage localization (i.e., fully localized macro-crack phase). To achieve this goal, several drawbacks of standard INL and GNL formulations should be overcome:

- (i) *Damage initiation near a crack tip.* This is the shift of the maximum non-local equivalent strain far from the crack tip, leading to damage initiation problems [28]. This drawback will not be treated in this paper and is left for future works.
- (ii) *Damage attraction to the boundaries.* This is the gradual shift of the maximum damage value to the boundary of the domain. This is related to the truncated interaction domain for INL models or the symmetry imposed by the zero flux condition on the boundary for GNL models. However, one expects that the response should become local in this case (vanishing non-local interactions) [27, 35].

³The physical meaning of the homogeneous Neumann boundary condition is still an open question, and further discussions may take place [44–46].

- (iii) *Damage diffusion.* Upon strain localization, the coalescence of micro-cracks into a macro-crack should induce a discontinuity in the displacement field. Classic models do not enable describing such a transition, as damage is diffused in a large zone. Thus, the internal length should account for this effect and be modified throughout the damage process [30]. In the numerical context of this work, damage diffusion will be considered to occur when $D \approx 1$ in more than one FE. Conversely, a perfectly localized damage profile is considered when $D \approx 1$ in just one FE.

Several non-local models with evolving non-local interaction distances depending on the mechanical field (stress, damage ...) were proposed in the literature to overcome these limitations. This work considers three different non-local models with evolving internal length. In particular, attention is focused on a Stress-Based integral Non-Local (NLSB) formulation [31], and on the Eikonal Non-Local (ENL) formulation [37, 38] (in both integral and gradient forms).

2.3.1. Stress-based non-local damage model

The NLSB model [31] takes into account the influence of the stress field at point y in the computation of the weight function at point x . Denoting by f_t the material tensile strength, this is done by replacing the characteristic length in (5) by:⁴

$$l_{c,xy} = \rho_{\text{fac}}(y)l_c \quad \rho_{\text{fac}}(y) = \frac{|\sigma(y)|}{f_t}. \quad (9)$$

According to (9), the influence factor $\rho_{\text{fac}}(y)$ is equal to zero when y belongs to a free boundary, which corresponds to the zero normal stress condition. Consequently, the weight computed between a given point inside the domain and another one on the free edge is null (i.e., no interactions are modeled). Moreover, if $\rho_{\text{fac}}(y) = 1$ the classical INL formulation is recovered.

2.3.2. Eikonal non-local damage model

The ENL damage model [37] is a geometric extension of the non-local internal time model introduced by [34]. In this approach, non-local interactions are supposed to behave as waves propagating from one point to the others of the damaged domain: the higher the time needed for wave propagation, the lower the interaction between the considered points. Consequently, the time needed to propagate information (interaction) between points increases when damage occurs and eventually tends to infinity when damage tends to the unity. Pijaudier-Cabot *et al.* [35] proposed a similar non-local model, where an attenuation function is used to describe the influence of damage on the non-local interactions.

Integral-type formulation (ENLI). In a multi-dimensional context, the ENL model leads to consider that damage deforms the space in which interaction distances are computed [37, 38]. It is supposed that non-local interactions between a point x and any other point y belonging to Ω depend on an effective distances field $\tilde{l}_{xy}(y)$ which is the solution of an eikonal equation with a damage-dependent Riemannian metric field. In a 1D context, the eikonal equation to be solved $\forall x \in \Omega$ can be written as:

$$\sqrt{1 - D(y)} \left| \frac{d\tilde{l}_{xy}(y)}{dy} \right| = 1 \quad \text{with } \tilde{l}_{xy}(y = x) = 0. \quad (10)$$

⁴In the general multi-dimensional case, ρ_{fac} is the radial coordinate of an ellipsoid associated with the stress state of a nearby point y . Thus, this model naturally solves boundary effects issues, given that at the presence of a free boundary, the stress state is considered to modify non-local interactions.

Equation (10) can be integrated analytically,⁵ and the effective distance between points x and y reads [37, 47]:

$$\tilde{l}_{xy} = \int_{\min(x,y)}^{\max(x,y)} \frac{dy}{\sqrt{1-D(y)}} > l_{xy}. \quad (11)$$

According to such an approach, the main modification with respect to the INL formulation is the use of the \tilde{l}_{xy} instead of l_{xy} in (5). Recent works have shown that the ENLI approach is suitable for modeling strain localization processes [37, 38, 40, 47].

Gradient-type formulation (ENLG). An equivalent gradient-enhanced ENL damage model (ENLG) was also formulated in [37]. In 1D tension, the modified version of the Helmutz's equation (6) to be solved to compute the non-local strain field is:

$$\bar{e}(x) - c\sqrt{1-D(x)} \frac{d}{dx} \left(\sqrt{1-D(x)} \frac{d\bar{e}(x)}{dx} \right) = e(x) \quad \text{in } \Omega \quad \text{with} \quad \frac{d\bar{e}(x)}{dx} = 0 \quad \text{on } \partial\Omega. \quad (12)$$

Similarly to (8), the variational formulation of the ENLG problem reads:

$$\int_0^L c\sqrt{1-D} \frac{d\bar{e}}{dx} \frac{d\eta}{dx} dx + \int_0^L \frac{\bar{e}\eta}{\sqrt{1-D}} dx = \int_0^L \frac{e\eta}{\sqrt{1-D}} dx \quad \forall \eta \in \mathcal{E}. \quad (13)$$

The latter is basically the same equation obtained for the classical GNL model, with the additional term $\sqrt{1-D}$. In the ENLI formulation, this term appears in (10) and is related to the determinant of the Riemannian metric. Indeed, damage tends to increase the effective distances. When it tends to the unity, the effective distance between two points separated by the highly damaged zone tends to infinity [37, 38, 47], so that the non-local interaction between the considered points vanishes. To the authors' knowledge, no numerical implementation of such an approach exists in the literature.

3. One-dimensional dynamic problem

The spalling test (Figure 1) will be used to underline some typical drawbacks and advantages of different regularization models. As already done in [27, 31], this test is simulated to study boundary effects and localization properties of modified non-local formulations. A precise review of this problem was also presented in [48], where the advantages of considering a modified interaction-based non-local approach [49] were presented.

Description of the spalling test. Experimentally, spalling can be obtained with a modified Hopkinson test (Figure 1). The experimental setup consists of an input striker, an incident bar, and the specimen. After being transmitted to the specimen, the compression wave starts to reflect as a tensile wave at the free boundary. For a strain-softening material, when the sum of the compression and tensile contributions to the elastic wave is greater than the material tensile strength, a fully localized cracking occurs. Thus, the spalling test is an excellent tool for simulating strain localization and evaluating the properties of damage models.

3.1. Weak form of the dynamic equilibrium problem

Let us consider a 1D domain $\Omega = [0, L]$, with an imposed Neumann condition (external impulsive force) on $\partial\Omega_F = \{x = L\}$. The other boundary is stress-free.

⁵This is not the case in a more general multi-dimensional setting, in this case, numerical integration methods (e.g., the Fast-Marching approach) are needed. The first FE implementation of the ENL model in two dimensions was proposed by Rastello *et al.* [38].

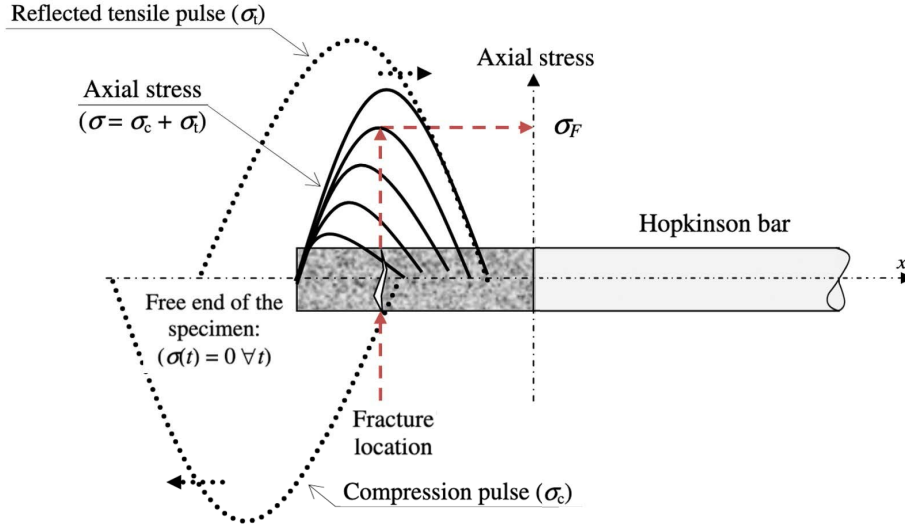


Figure 1. Illustrative scheme of the spalling test with a Hopkinson bar [26].

3.1.1. Variational problem

Let us introduce the following admissibility spaces:

$$\mathcal{U} = \{u \mid u(x, t) \in H^1(\Omega), u(x, t) \in H^2(I), u(x, t = 0) = 0 \forall x \in \Omega\} \quad (14)$$

$$\mathcal{V} = \{v \mid v(x) \in H^1(\Omega), v(x, t) = 0 \text{ on } \partial_u \Omega\}, \quad (15)$$

where $H^n(\cdot)$ denotes the n -order Sobolev space over a domain and $I = [0, T]$ is the time interval.

Neglecting body forces, the variational dynamic equilibrium problem to be solved consists in finding $u = u(x, t) \in \mathcal{U}$ such that:

$$\int_0^L \sigma(u) \epsilon(v) dx + \int_0^L \rho \ddot{u} v dx = T_d(t) v(L) \quad \forall v \in \mathcal{V}, \quad (16)$$

where $\ddot{u} = \partial^2 u / \partial t^2$ is the acceleration field, ρ is the mass density, and $T_d(t)$ is the applied traction (force per unit area) on $\partial_F \Omega$.

3.1.2. Time discretization

The equation (16) is solved for each time instant $t \in I$ after time discretization (e.g., using the Newmark scheme). In this paper, the explicit central difference scheme is employed. Accordingly, the time interval is discretized as $t \rightarrow t_n \in [0, T = n_t \Delta t]$ with $n \in \llbracket 1, n_t \rrbracket$ and Δt the time step. At time t_{n+1} , one thus solves for \ddot{u}_{n+1} the time discretized variational equation:

$$\int_0^L \rho \ddot{u}_{n+1} v dx = T_{d,n+1} v(L) - \int_0^L \sigma(u_{n+1}) \epsilon(v) dx \quad \forall v \in \mathcal{V}, \quad (17)$$

where:

$$\begin{cases} u_{n+1} = u_n + \Delta t \dot{u}_n + \frac{1}{2} \Delta t^2 \ddot{u}_n \\ \dot{u}_{n+1} = \dot{u}_n + \frac{\Delta t}{2} (\ddot{u}_{n+1} + \ddot{u}_n). \end{cases} \quad (18)$$

In (16) and (18), subscripts n and $n+1$ are used to denote quantities computed at time instants t_n and t_{n+1} . The same nomenclature will be adopted in the remainder of the text.

Such a method is suitable for non-local computations in a dynamic context. Moreover, there is no need to apply nonlinear iterative procedures such as Newton–Raphson.

3.1.3. Space discretized problem

To solve the variational equation (16), the computational domain Ω is discretized into a FE mesh Ω^h containing n_{el} linear bar elements of constant length h . Accordingly, the displacement field is approximated as a function of the nodal displacements through the elementary shape functions. Stress and strains are computed at the quadrature points of the FEs. A single integration point located at the center of the FE is considered for linear elements. We denote by \mathcal{G} the set of the $n_{gp} = n_{el}$ integration points of Ω^h .

3.1.4. Constitutive model

The stress is evaluated according to the constitutive relation (1). For the numerical simulations of this paper, the history function driving the damage evolution is defined as the historical maximum of the non-local strain. For the integration point x_i , it is computed as $\kappa_i = \kappa(x_i) = \max_t(\kappa_0, \bar{e}_i)$ with $\bar{e}_i = \bar{e}(x_i)$. Damage grows according to (2).

3.2. Non-local fields computation

The non-local field (\bar{e}) is computed following one of the methods introduced earlier: INL, GNL, ENLI, ENLG or NLSB. In a FE context, one computes the non-local strain field to evaluate damage, and thus the stress, for each Gauss integration point of Ω^h .

3.2.1. Integral non-local methods

For a given Gauss point $x_i \in \mathcal{G}$, the non-local equivalent strain $\bar{e}_i = \bar{e}(x_i)$ is obtained as:

$$\bar{e}_i = \frac{\sum_{j=1}^{n_{gp}} e_j \phi(l_{ij}^*, l_{c,ij}^*)}{\sum_{j=1}^{n_{gp}} \phi(l_{ij}^*, l_{c,ij}^*)}, \quad (19)$$

where $e_j = e(x_j)$ and we exploited the fact that all FEs have the same size.

The main difference between the different integral-type non-local formulations discussed earlier is in the way how l_{ij}^* and $l_{c,ij}^*$ are computed.

INL. In the standard INL formulation, $l_{ij}^* = l_{ij} = |x_i - x_j|$ and $l_{c,ij}^* = l_c$.

NLSB. In the NLSB damage model [31], the weighting function depends on the stress field. In the explicit 1D implementation of this work, the modified internal length $l_{c,ij}^*$ is directly computed from the stress ($\sigma_{j,n} = \sigma_n(x_j)$) at the previous time step, whereas $l_{ij}^* = l_{ij} = |x_i - x_j|$.

The following steps are needed to perform the computation. The coefficient $\rho_{fac,j} = \rho_{fac}(\sigma_{j,n})$ is first computed for $x_j \in \mathcal{G}$ as:

$$\rho_{fac,j} = \begin{cases} |\sigma_{j,n}|/f_t & \text{if } |\sigma_{j,n}|/f_t \leq 1 \\ 1 & \text{otherwise.} \end{cases} \quad (20)$$

The modified characteristic length is then computed as:

$$l_{c,ij}^* = \begin{cases} \rho_{fac,j} l_c & \text{if } \rho_{fac,j} l_c \geq h \\ h & \text{otherwise.} \end{cases} \quad (21)$$

Finally, the non-local weight $\phi(l_{ij}, l_{c,ij}^*)$ is computed and used in (19).

ENLI. For the ENLI formulation, the damage-dependent interaction distances need to be computed. In (19), $l_{c,ij}^*$ is taken equal to l_c whereas l_{ij}^* is the effective distance $\tilde{l}_{i,j}$ between the two integration points x_i and x_j [40, 47]. Numerically, the integral (11) is replaced by a finite sum over all the points in the interval $[x_i, x_j]$.

Jirásek and Desmorat [40] proposed two schemes to perform the integral calculations: a simple trapezoidal rule such that $\sqrt{1-D}$ is element-wise constant and a modified approach assuming that damage is linear between two adjacent integration points. As shown in [47], the first approach has better localization properties, especially when combined with appropriate path-following algorithms [50].

According to the latter approximation, $l_{ij}^* = \tilde{l}_{i,j}$ is computed as:

$$\tilde{l}_{i,j} = \tilde{l}_{i,j-1} + \frac{h}{2} \left(\frac{1}{\sqrt{1-D_{j-1,n}}} + \frac{1}{\sqrt{1-D_{j,n}}} \right), \quad x_j > x_i, \quad (22)$$

where $D_{j-1,n} = D_n(x_{j-1})$ and $D_{j,n} = D_n(x_j)$.

3.2.2. Gradient-enhanced non-local methods

GNL. Equations (8) and (16) need to be solved as a coupled problem [51].⁶ Accordingly, the non-local strain field and the corresponding trial field (η) are discretized by appropriated shape functions. Many authors argued that it was necessary (or at least advisable) to employ displacement shape functions one order higher than those used for the non-local field [16, 53]. Indeed, using the same interpolation functions for the displacement and the non-local strain may lead to stress oscillations. However, Simone [51] showed that the gradient-enhanced damage problem should not be considered as a mixed problem (i.e., the Babuska–Brezzi condition does not apply) but rather a coupled one. Consequently, the interpolation functions chosen for the two unknown fields are not related and can be taken simply as linear-linear.

ENLG. Similarly to the standard GNL formulation, the governing equations (13) and (16) are solved as a coupled problem. To preserve the explicit feature of the present FE implementation, the Helmholtz equation (13) is computed with $D_n = D(\kappa_n)$. This is consistent with the choice made for the ENLI formulation.

3.2.3. More numerical details

Computation of evolving non-local interactions. For all the non-local models with evolving distance models, damage and stress are always one step delayed with respect to the displacement, given the choice to explicitly compute the non-local evolving interactions. This is in agreement with the quasi-static implementations developed by Rastello *et al.* [38] for the ENLI model, and by Giry *et al.* [31] for the NLSB model.

Equivalent strain interpolation for the GNL and ENLG models. For both gradient models, once the nodal non-local equivalent strain field is obtained at time t_{n+1} , the shape interpolation functions are applied to obtain the corresponding values at the Gauss points.

Dealing with the case of D tending to the unity. Generally, FE solvers for CDM problems limit damage growth to a certain fixed quantity D^* at the Gauss quadrature point while integrating the material behavior law (updating internal variables, computing the stress, and evaluating the elemental stiffness matrix). In nonlinear quasi-static analyses, where the stiffness matrix need to be inverted to compute the solution displacement field, D^* is chosen in a way that the stiffness matrix does not become singular.

In the case of the explicit time integration scheme of this work, there is no need to inverse the stiffness matrix for the computations. Thus, D^* is taken as close as possible to unity, to avoid

⁶This is similar to implementing thermo-elasticity equations with an equivalence between nodal temperatures and nodal non-local strains [48]. This simple analogy allows to easily incorporate non-local gradient formulations (or even phase-field models) in commercial FE analysis software (see, e.g., [52]).

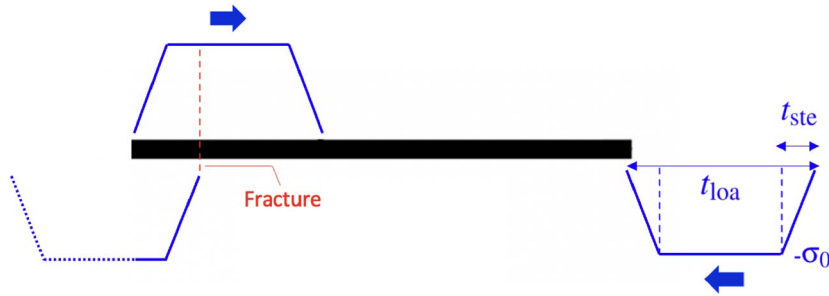


Figure 2. 1D bar model of the spalling problem. A compression signal comes from the right and is reflected in tension when it reaches the free left boundary.

problems when computing the effective distances field for ENLI. This is automatically handled by the library `numpy` in Python. Machine precision is taken into account by setting $1/\sqrt{1-D^*}$ equal to `numpy.inf`, which is equivalent to the largest number that can exist with the available memory in the machine. Then, when evaluating the Gauss weighting function with $\tilde{l}_{i,j} = \text{numpy.inf}$, the Python code will return 0. This is in agreement with the fact that non-local interactions should vanish upon damage localization as stated by the ENLI model. As a consequence, in this case, D^* can be taken as high as the machine supports.

4. Results and discussion

The spalling experiment will be treated hereafter. To limit numerical noise at the introduction of the loading, a linear ascending and descending compression stress is applied during a finite time t_{ste} (Figure 2). The total loading time is t_{loa} and the final stress applied is $-\sigma_0$. A signal length l_0 can be related to the loading time by $l_0 = t_{loa}c_p$, where $c_p = \sqrt{E/\rho}$ denotes the longitudinal wave velocity. Choosing $\sigma_0 \geq f_t$ leads to strain localization and therefore damage develops. The main advantage of comparing non-local models studying this problem is the facility to control where localization occurs; the fracture will be located exactly at a distance $l_{spal} = l_0/2$ from the free edge.⁷

The material parameters used for the simulations are the same as those in [27, 31], i.e., $E = 1$ MPa, $\kappa_0 = 1$, $B = 2$, $L = 25$ cm, $f_t = 1$ MPa, $\sigma_0 = \alpha f_t$, $l_c = 3$ cm and $\rho = 1$ kg/m³. Here, $\alpha \geq 1$ is a constant parameter chosen arbitrarily to induce damage. The simulation time is set to $T = 1.5L/c_p = 0.3750$ ms. Time step is chosen as $\Delta t = \Delta t^{crit}/2$, where Δt^{crit} is the critical time step related to the explicit scheme and depends on the mesh size. A study of the influence of Δt on the obtained responses for the considered non-local formulations is presented in Appendix A.

4.1. Boundary effects and damage diffusion with fixed interactions models

Let us first consider the standard INL model. Different mesh discretizations (with n_{el} ranging from 100 to 400) are used in computations to study mesh sensitivity of the obtained responses. A sufficiently large loading time is considered. In particular, $t_{loa} = L/c_p$ and $t_{ste} = 0.05t_{loa}$. This means that $l_0 = L$; therefore, one should expect a damaged band centered in the middle of the bar.

⁷Bažant and Belytschko [54] studied the same problem with the difference that two tensile waves would propagate from each free end. This implies that the sum of these localizes strain in the middle of the bar in the case of strain-softening materials. An exact analytic unique solution exists for given boundary and loading conditions, which means that treating strain-softening materials in a continuum framework is indeed possible.

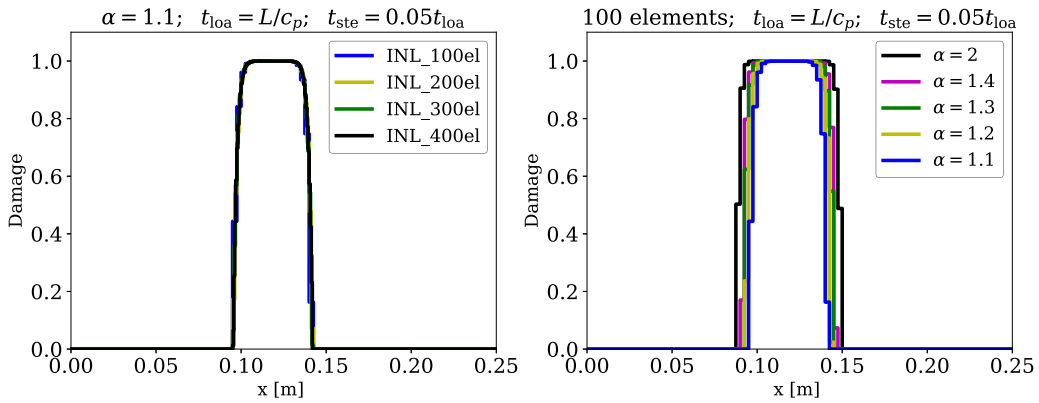


Figure 3. INL damage model—convergence of the damage profile upon mesh refinement (left) and influence of the loading parameter α on damage diffusion upon damage localization (right).

4.1.1. Damage regularization and diffusion

Figure 3 (left) shows the damage distribution along the bar obtained for $\alpha = 1.1$. As expected, damage reaches its maximum close to the middle of the bar ($x = L/2$) but it diffuses on a bigger zone than one FE. Moreover, the INL model regularizes the response as the damage profiles converge upon mesh refinement.

The choice of α may modify the obtained response. Figure 3 (right) shows the damage profiles computed for different values of α . For a fixed loading duration, changing α changes the strain rate, which would affect the non-local averaging. This is also the case for the other non-local models studied in this work. However, the presented results can provide information on the main features of the responses provided by the different formulations studied in this work (when compared for a given α).

The time evolution of the damage field on the bar is shown in Figure 4 for $\alpha = 2$. Damage first takes its maximum value in only one FE, then starts to diffuse in the surrounding FEs. At the end of the simulation, damage equals unity in a quite large zone. As already pointed out in [30], the non-local field still evolves outside the localization zone due to strain intensification. Non-local interactions are even allowed to take place between points separated by highly damaged zones, as the material state is not taken into account in the averaging process.

4.1.2. Boundary effects

Damage attraction to the free boundary is observed when $l_{spal} < l_c$. To highlight this problem, a few values of l_0 are used with a FE mesh of 100 elements. Here, α is set equal to 2 to observe a damaging process up to failure (i.e., $D \approx 1$ in at least one FE).

INL formulation. For values of $l_{spal} < l_c$, damage is gradually attracted by the boundary and takes its maximum at the free edge (Figure 5). This effect is related to the fact that the interactions introduced through the non-local weight function ϕ only depend on the euclidean distance between points. Near a free boundary, the interaction domain is truncated; therefore the non-local weights computed for these points are bigger. In this case, this results in an infinitely small spalling thickness: the distance from the free edge to the point of maximum damage is nil ($D \approx 1$ shifts to the free boundary). As shown in Figure 5 (right) damage diffusion is also present in the

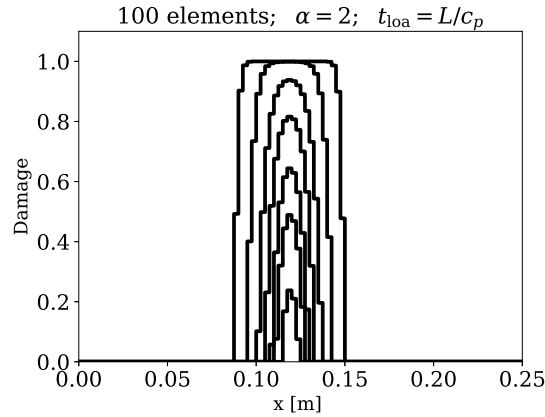


Figure 4. INL damage model—damage evolution through time for $l_0 = 25$ cm.

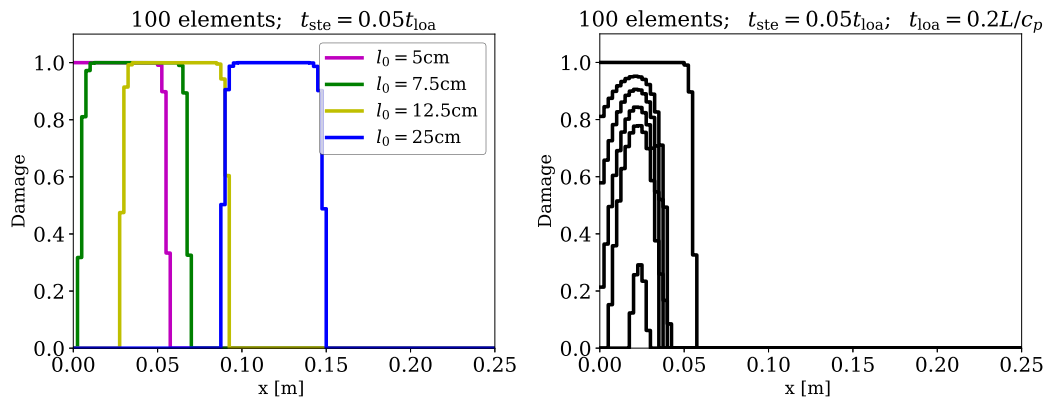


Figure 5. INL damage model—influence of l_0 on damage attraction (left) and its evolution through time (right).

last steps of the computation. As expected, this indicates that the transition from diffuse damage to fully localized damage cannot be conveniently described with this model.

INL vs. GNL formulations. This result may also be extended to the classical GNL model, as a zero flux condition is applied to solve the non-local strain diffusion equation. Figure 6 illustrates the equivalence between GNL and INL formulations. The two models provide very similar results. The small differences between them are certainly related to the fact that they are equivalent *stricto sensu* only when an infinite domain is considered for a Green's weight function [44]. Mesh refinement may slightly reduce the differences between the observed responses (see Figure 6).

4.2. Boundary effects and damage diffusion with evolving interactions models

In this section, a comparison of the non-local models with evolving interactions is performed. Two different loading cases are considered:

- (i) **Loading case A**—Damage localization far from the free boundary ($l_{\text{spal}} = 6.250$ cm $> l_c$):
 $t_{\text{loa}} = 0.5L/c_p$.

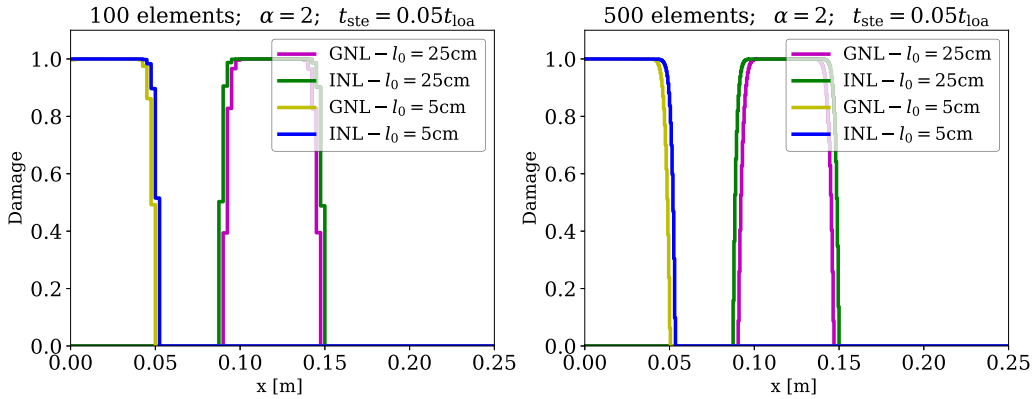


Figure 6. INL and GNL damage models—equivalence between the two formulations for 200 and 500 FEs.

- (ii) **Loading case B**—Damage localization near the free boundary ($l_{\text{spal}} = 2.500 \text{ cm} < l_c$):
 $t_{\text{loa}} = 0.2L/c_p$.

In all the cases studied, t_{ste} is assumed equal to $0.1 t_{\text{loa}}$. The effect of the strain rate on the localization process is studied by modifying the loading parameter α . Since changing t_{ste} has almost the same effect, such parameter is taken constant for the sake of simplicity and conciseness of presentation.

4.2.1. Damage diffusion (loading case A)

Integral formulations. The loading case A is simulated for two meshes containing 100 and 500 linear FEs and $\alpha = 1.5$. Figure 7 (left) compares the damage profiles computed using the INL, NLSB, ENLI, ENLG, and GNL damage models at time $t = T$. Damage diffusion is observed for the INL model, but is much smaller for the NLSB and ENLI formulations. As expected, the ENLI model allows for a better description of the damage localization process, since damage concentrates on only one FE as non-local interactions vanish when damage localizes. Conversely, damage is spread over three FEs for the NLSB model. Figure 7 (right) gives the same results for a mesh with 500 FEs. Here, the ENLI formulation spreads damage over three FEs, whereas the NLSB model spreads it over nine FEs.

Integral vs. gradient formulations. The damage profile computed with the GNL model is thinner than the one obtained using the INL formulation. The ENLG model provides almost the same damage profile as the ENLI formulation, except for highly damaged zones (Figure 7 (right)). Indeed, the damage is spread over a large region (its width is still smaller than the one computed by the classical non-local models). This is an unexpected behavior, given that the ENLG formulation is an approximation of the ENLI model and therefore should give similar results. However, the damage diffusion is clearly reduced upon mesh refinement for the ENLG formulation (Figure 7).

From Figure 7, one can also see that the widths of the damaged zones for the models with evolving interactions are smaller than those given by the classic formulations. Moreover, the models with fixed distances propagate the damage front with passage of time even after damage attains unity, as we will see later on. Thus, widths of the damaged area (i.e., total of elements where $D > 0$) are not constant for these models and tend to increase (see Table 1). Differently, models with evolving distances do not show an evolution of the damage zone when comparing profiles for $D_{\text{max}} = 0.99$ and $D_{\text{max}} \rightarrow 1$. In this situation, the ENLG and ENLI formulations give

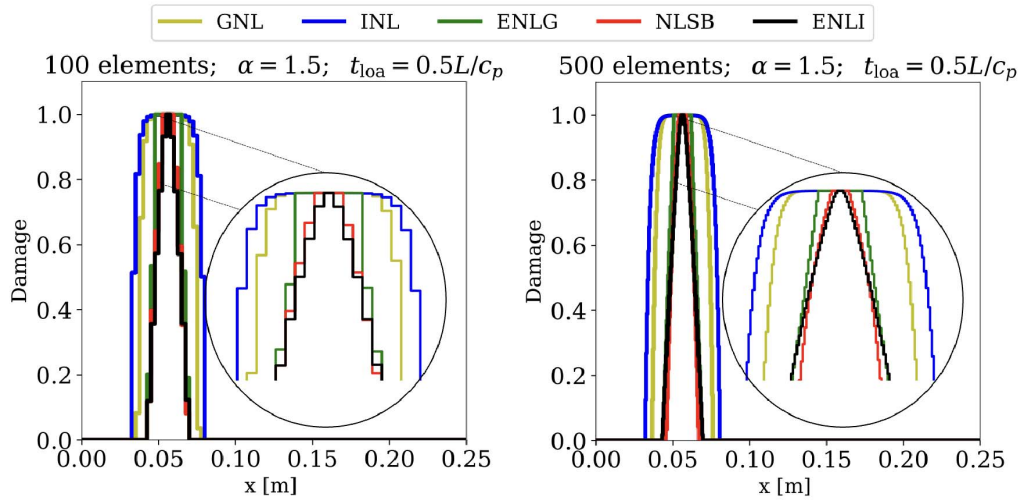


Figure 7. INL, GNL, NLSB, ENLI, and ENLG damage models—comparison between all the models studied for two meshes with 100 and 500 FEs.

Table 1. INL, GNL, NLSB, ENLI, and ENLG damage models—width of the damaged zones for each non-local model for a mesh with 500 FEs

Non-local model	INL	GNL	ENLI	ENLG	NLSB
Width (% l_c) of the damaged area when $D_{\max} = 0.99$	157	120	90	87	73
Width (% l_c) of the damaged area when $D_{\max} \rightarrow 1$	170	133	90	87	73

very similar widths, and the NLSB model shows the smaller one. Smaller damaged zones are indeed expected for the evolving interaction approaches. In the case of the ENLI and ENLG models, the interactions begin to evolve since damage appears, and vanish upon damage localization. For the NLSB model, the stress field is reduced when damage occurs, leading to an evolution of the internal length. Furthermore, one may expect these widths to not evolve after damage localization on one FE, as interactions between points through highly damaged zones should not occur.

Influence of the strain rate. Parameter α influences the damage diffusion process for all the considered models. In any case, evolving interaction models give more representative results of the degradation process. The damage profiles obtained by these approaches are almost insensitive to mesh refinement. The main difference between the formulations is their capability to describe damage localization, which ENLI better simulates. Figure 8 allows quantifying better the influence of α on the damage diffusion mentioned above for a mesh with 500 FEs. The number (N_α) of FEs where diffusion occurs is dependent on the value of α for all the models, but the influence of such a parameter is more pronounced for the INL and GNL models.

4.2.2. Boundary effects (loading case B)

Another usual situation for which one may compare non-local models is when the damaged band is located near a free boundary.

Integral vs. gradient formulations. Figure 9 shows the results for the INL, ENLG, ENLI and NLSB models for $\alpha = 2$. No damage attraction from the boundary is observed for the ENLG and NLSB formulations. In those cases, the boundary effect does not occur, so it is possible to determine the spall location numerically. Contrarily, the ENLI formulation shows a minor boundary effect

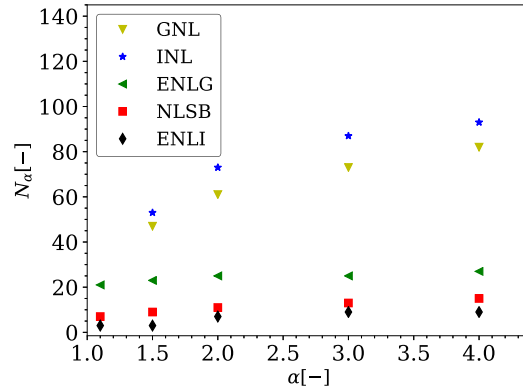


Figure 8. INL, GNL, NLSB, ENLI, and ENLG damage models—influence of α on the size of the localization zone for a mesh with 500 FEs.

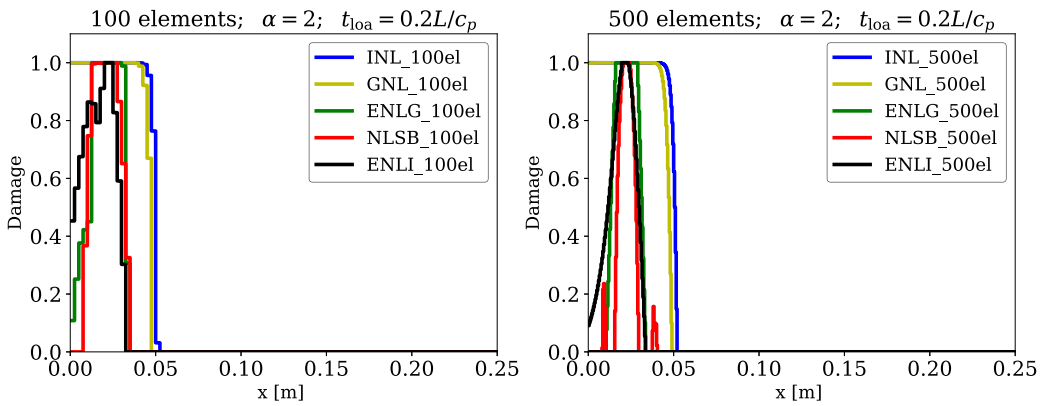


Figure 9. INL, GNL, NLSB, ENLI, and ENLG damage models—comparison of damage profiles near the boundary for $\alpha = 2$.

compared to the INL model, but some influence on its response is still observed. Despite such a damage attraction, it is still possible to define the spall location for the ENLI formulation, as the fully damaged area does not reach the free edge.

Influence of the strain rate. Figure 10 shows the same results, but for $\alpha = 1.5$. Decreasing α reduces the damage diffusion for all the models. The boundary effect is also reduced for the INL and GNL models (for the given problem). However, the damage value at the free edge increases when reducing α from 2 to 1.5 for the ENLI formulation. In this situation, a minor parasite effect can also be observed for the ENLG model. The NLSB model does not show any boundary effect. Still, it exhibits a small region of minor damage (also for $\alpha = 2$) in the vicinity of the main damaged zone (see Appendix A for a better explanation of this effect). Figure 11 shows the comparison between all the non-local models regarding the influence of α on the boundary effect considering only the cases where damage reaches the unity. Finally, although the ENLG formulation shows damage diffusion, the model gives more reliable results regarding the maximum damage location when the bar is submitted to higher strain rates than the ENLI model.

The spall location can be numerically estimated without any problem despite minor damage diffusion or attraction for the models with evolving interactions. One should consider, for example, the middle of the region where damage attains its maximum and compute its distance to

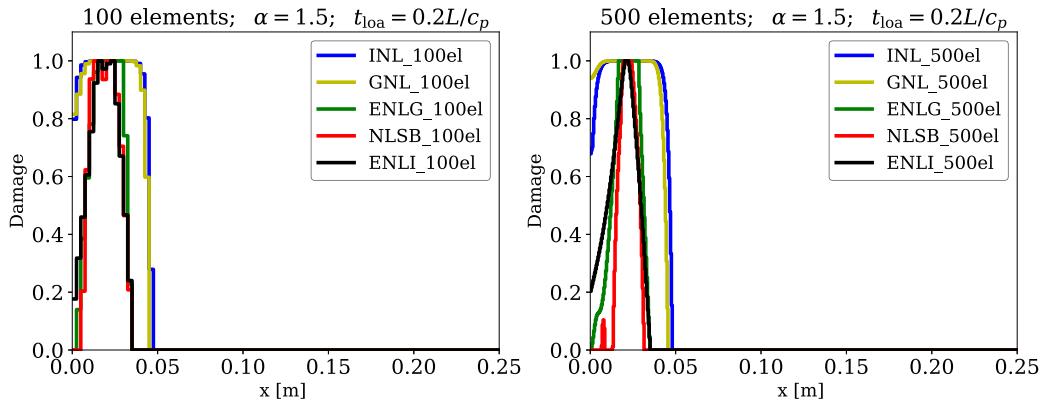


Figure 10. INL, GNL, NLSB, ENLI, and ENLG damage models—comparison of damage profiles near the boundary for $\alpha = 1.5$.

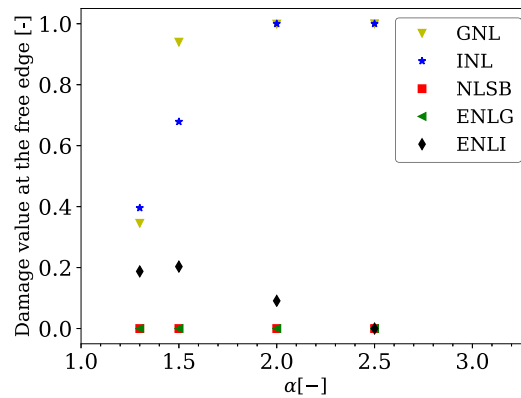


Figure 11. INL, GNL, NLSB, ENLI, and ENLG damage models—comparison regarding the effect of α on the damage value on the boundary for a mesh with 500 elements.

the free edge. This is not possible with the classic non-local formulations, as maximum damage inevitably shifts to the free edge during the simulation, which is shown in detail in the following.

4.3. Further analyses: differences observed between models with evolving interactions

Given the results presented in the previous section, a more specific analysis may be performed to highlight better and justify the differences between the different formulations with evolving interaction distances. In particular, it is essential to understand the differences observed between the ENLG and ENLI models regarding damage diffusion, as they should give similar results. Moreover, an overall comparison between the ENLG, ENLI, and NLSB formulations is also necessary. For this purpose, one may compare the dissipated energies and the evolution of the free-surface/face velocity (i.e., the velocity registered on the free edge of the ejected part of the specimen, which corresponds to the spalling phenomenon). The standard INL and GNL formulations are also analyzed for completeness.

A semi-analytical study is also developed in Appendix B to illustrate the differences between the integral models in the computation of the non-local strain field. The observed behaviors

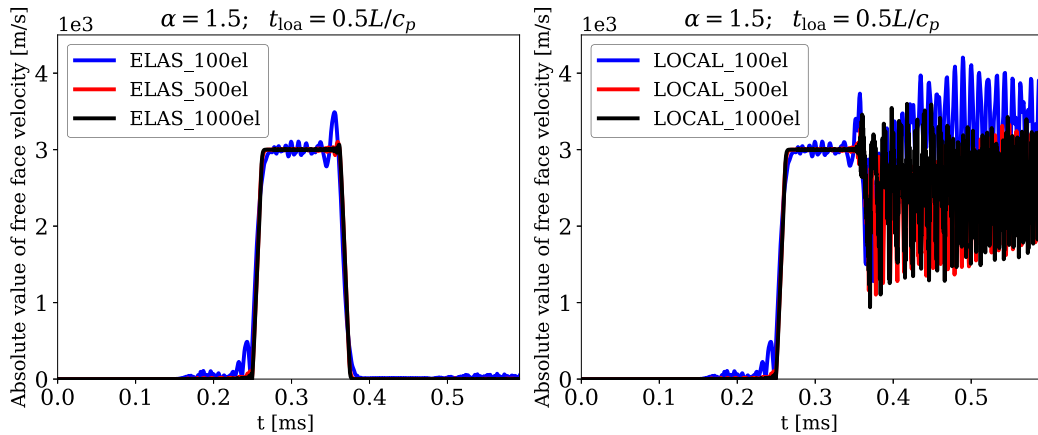


Figure 12. Linear elastic (left) and local damage (right) models—Free-surface velocity profiles.

are in agreement with the numerical results given in the following and may highlight how these models deal with existing or newly created boundaries.

4.3.1. Free-surface velocity

As already explained, when damage attains unity in the bar, the left part of the bar is ejected. The free-face velocity (at $x = 0$ cm), i.e., the so-called ejection velocity, is a good indicator of regularization and can be used to highlight the differences observed between the models studied. To this end, let us consider once again the loading case A of Section 4.2.1. The same material parameters as in the previous examples are used, and $\alpha = 1.5$ for all the models. It should be noticed that, for the numerical examples of this work, the input signal comes from the right to the left, so the free-surface velocity has a negative sign. For better comprehension, the absolute value of this velocity will be taken for the analyses presented hereafter. Comments are given using only the term “velocity”, but one may consider that this refers to its absolute value.

Elastic and local damage response. The free-surface velocity obtained for a linear elastic material model is shown in Figure 12 (left). As expected, convergence is obtained upon mesh refinement. Moreover, one may only see the input signal which is reflected on the free edge, given that no damage occurs. If a local damage model is considered (see, e.g., Section 2.1), damage will take place at a certain distance from the free boundary (i.e., the spalling distance). Figure 12 (right) shows the free-surface velocity profile obtained for a local damage model. In this case, mesh dependency is clearly observed after the maximum velocity value is reached.

Models with fixed interaction distances. In the case of the INL and GNL models, the free-surface velocities computed for different meshes are shown in Figure 13. As expected, both models give similar results, but some differences exist after the first reflection occurs on the damaged zone. In both cases, one may see the subsequent periodic signals arriving at the free edge. However, the signal periods reduce after each round trip between the free surface and the damaged zone. This indicates that the damage profile is still evolving after damage reached unity in the middle of the damaged band. Due to damage diffusion, the velocity also attains a limit point when time passes, but this condition arrives sooner for the GNL model than for the INL one.

The evolution of the GNL and INL damage profiles is given in Figure 14. One can see that for the GNL model (Figure 14 (left)), damage is progressively spread and attracted by the boundary

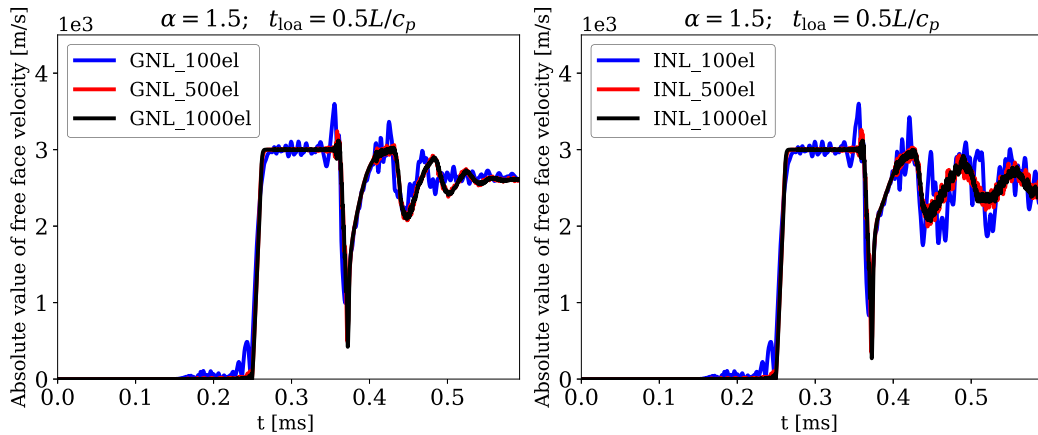


Figure 13. GNL (left) and INL (right) damage models—mesh convergence of the free-surface velocity response.

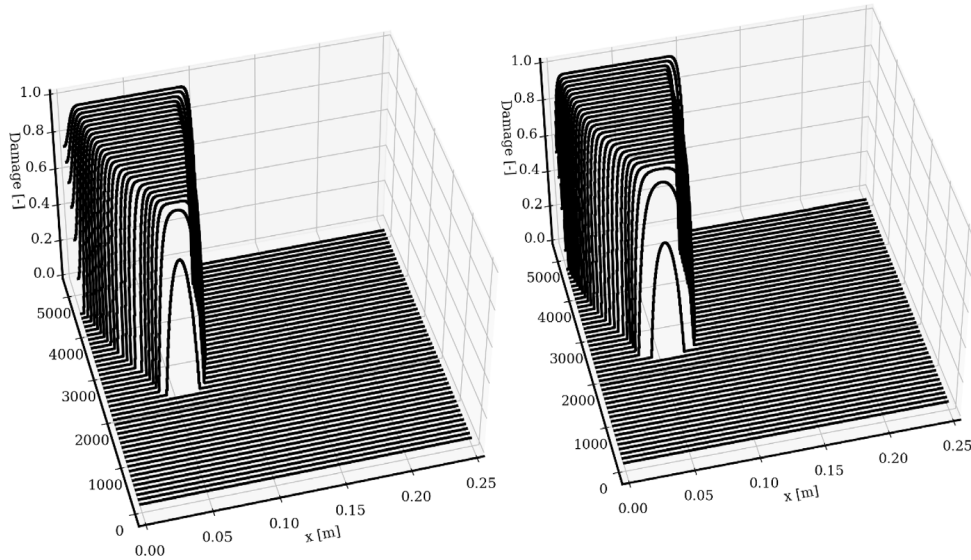


Figure 14. GNL (left) and INL (right) damage models—evolution of the damage profile through the simulation.

and reaches a considerable value (still smaller than 1) at the end of the simulation. This attraction is less pronounced for the INL model (Figure 14 (right)), which explains why the reflections between the free surface and the damage zone are more pronounced for such a model. Indeed, the spalling distance is reduced by the damage attraction to the boundary, which leads to the limit point in the free-surface velocity.

Models with evolving interaction distances. The limit point of the velocity is not observed for the models with evolving interactions (Figure 15). For the three considered formulations (ENLI, ENLG, and NLSB), the reflections due to spalling can be seen in the velocity profile. Here, the signal periods are not reduced, which indicates that there is no propagation of the damage front after damage localization. The convergence is only attained for more than 500 FEs, and

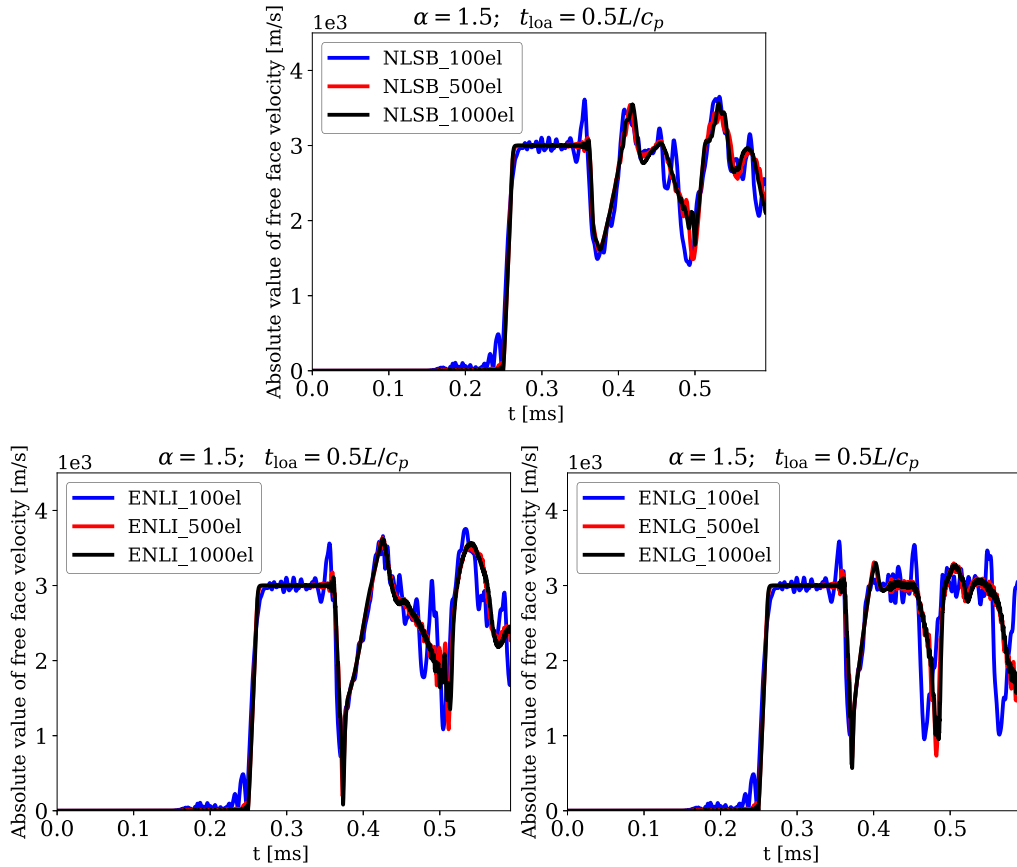


Figure 15. NLSB (top), ENLI (left), and ENLG (right) damage models—mesh convergence of the free-surface velocity response.

the velocities given by the three considered models are similar to the ones found in [55–57]. Significantly, the ENLG model shows the same type of velocity when compared to the simulations obtained for cohesive elements in [58].

Figure 16 shows the free-face velocity obtained for the ENLG model and damage evolution in the highly damaged FE. At the time instant corresponding to half of the input signal duration, already half of it is reflected as a tension loading. Thus, damage starts to evolve exponentially at this moment (Figure 16 (left)). After reaching unity, the rest of the signal coming from the boundary is reflected on the damaged zone, which induces some time after an increase in the free-surface velocity (pullback velocity). On Figure 16 (right), one can see the evolution of damage through time without propagation of the damage front.

A comparison of free-surface velocities given by all the models studied is given in Figure 17 for a mesh containing 1000 FEs. It is shown that the INL and GNL models give very similar results until 0.45 ms. Also, the NLSB and ENLI models show similar results in terms of spall signal but much different in terms of pullback velocity. These differences show that the models lead to different damage evolution rates.

4.3.2. Dissipated energy

To study how energy is dissipated for all the non-local models discussed in this work, loading case A is again considered assuming $\alpha = 1.5$. This choice ensures that damage attains unity for

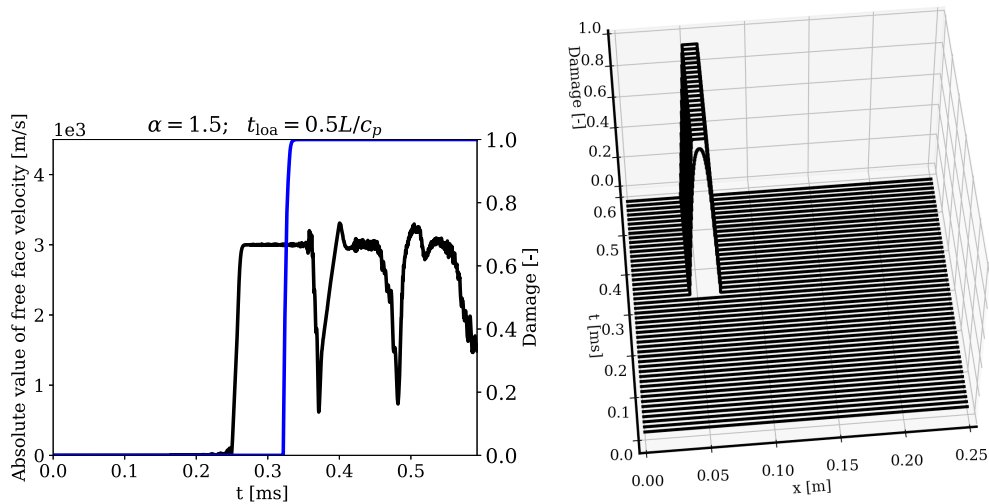


Figure 16. ENLG damage model—left: free-surface velocity (black) and damage evolution through time in the highly damaged FE (blue); right: evolution of damage through time.

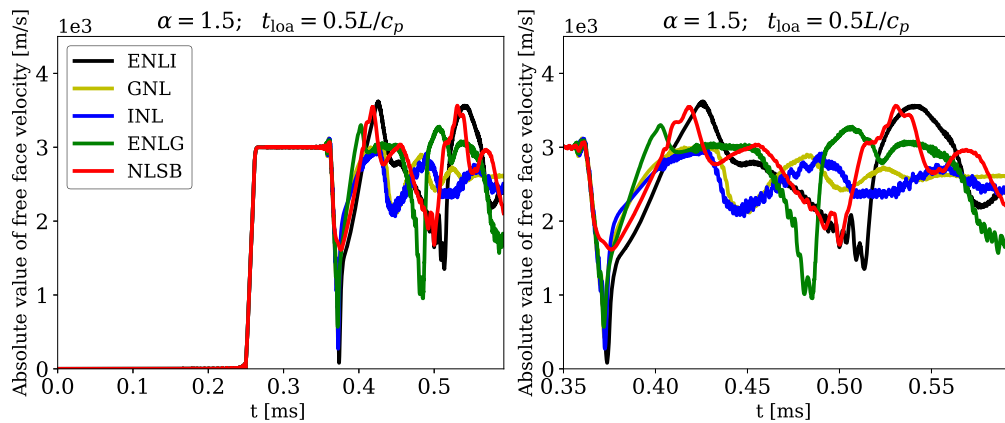


Figure 17. INL, GNL, NLSB, ENLI, and ENLG damage models—comparison of the free-face velocities.

all models. However, as shown in Sections 4.2.1 and 4.2.2, models with evolving internal length tend to spread damage over more FEs. In this work, the simple local expression of the intrinsic energy dissipation ($Y\dot{D}$) is employed.⁸ This latter quantity is computed for all time instants using a conventional numerical integration scheme and is accumulated over time. The profiles of dissipated energy along the bar are depicted in Figure 18 (left) for time $t = T$.

⁸Peerlings *et al.* [45] presented a thermodynamic formulation of the classic GNL approach, showing that the thermodynamic force Y remains unchanged compared to the local description. Same comments on this subject are given by Desmorat *et al.* [19], following also the framework proposed by Forest [59], regarding the micromorphic approach for damage. However, to our knowledge, there is no similar development for models considering evolving non-local interactions. It is still unclear if these formulations imply different expressions of Y . This subject will be studied better in the future.

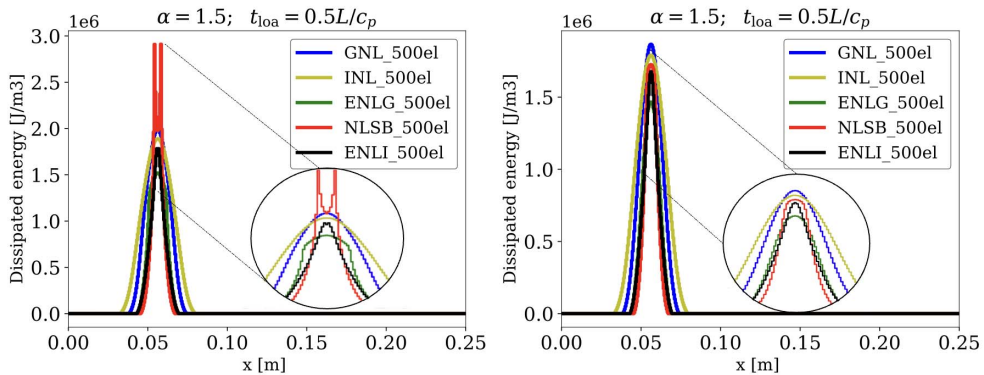


Figure 18. INL, GNL, NLSB, ENLI, and ENLG damage models—dissipated energy for $t = T$ (left) and when the maximum damage value reaches 0.99 (right).

Models with fixed distances. As expected, the widths of the zones where dissipation occurs are higher for the classical formulations than for the models with evolving interactions. The GNL model dissipates energy on a thinner region compared to the INL formulation.

Models with evolving distances. Despite the similarity observed in Figure 7 in terms of damage profiles obtained with all the formulations with evolving distances, one observes a huge difference in the dissipated energy between the NLSB model and the other formulations. The stress-based model continues to dissipate energy in the vicinity of the damage localization zone. Similarly, the ENLG formulation spreads the energy over a considerable zone compared to the ENLI model, thus reflecting the damage diffusion observed for this model.

Slightly different considerations can be done if one observes what happens at the time instant such that the first FE reaches a damage value of about 0.99 (Figure 18 (right)). In that case, models with evolving interactions give energy profiles that are similar between them but are different from those obtained through the classical approaches. Figure 19 shows the corresponding total dissipated energies (i.e., previous results integrated over the bar). The total dissipated energy is very similar between the approaches with evolving interactions and is almost the same for the ENLG and ENLI models when $D = 0.99$. For $t = T$ (end of the analysis), the ENLG and NLSB models show an increased dissipation, whereas the dissipation no more evolves for the ENLI model. The models with evolving non-local interactions dissipate much less energy than the formulations with fixed distances, which is expected as the widths of the damaged zones are smaller for the evolving distances approaches.

These considerations can also be extended to the damage profiles (Figure 20). All the evolving non-local models give almost the same damage profiles, except for some slight differences near the highly damaged zone. Damage diffusion is observed neither for the NLSB nor the ENLG formulations, as damage localizes in only one FE as for the ENLI model.

These considerations signal that some unexpected behavior occurs when damage tends to unity, especially for the ENLG formulation, which should not diffuse damage upon localization.

4.3.3. Damage evolution

The observed behavior can be better understood by examining the evolution of the damage field along the bar (Figure 21). In that case, the loading case A (see Section 4.2) is considered. Here, $\alpha = 1.1$ is assumed to ensure that a “correct” damage localization is modeled through the non-local models with evolving distances, even though, given this choice, damage does not attain unity for the classical non-local models.

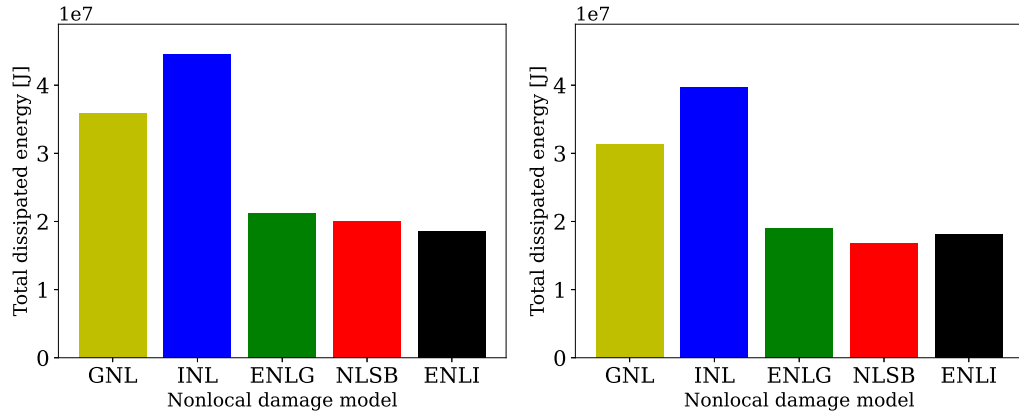


Figure 19. INL, GNL, NLSB, ENLI, and ENLG damage models—total dissipated energy for $t = T$ (left) and when damage value reaches 0.99 (right).

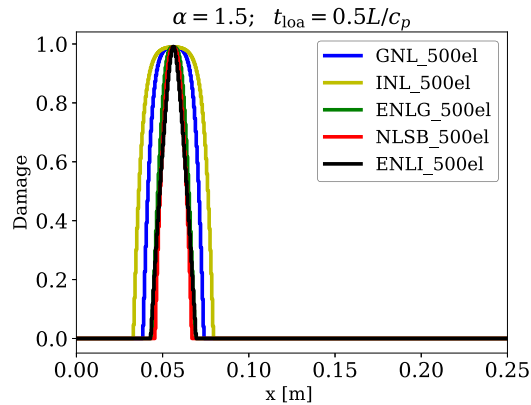


Figure 20. INL, GNL, NLSB, ENLI, and ENLG damage models—damage profiles when the first element reaches $D = 0.99$ for the different non-local model studied.

One observes that for low damage levels (e.g., close to the onset of damage, at $t = t_1$), all the models give essentially the same results except the NLSB formulation. At $t = t_2$, damage starts to grow faster than the other ones for the ENLG formulation, but still with a lower level when compared to the NLSB model. As expected, the ENLI model provides damage values similar to the GNL model but higher than those obtained through the INL formulation. Here, the main observation is that the damage levels for the gradient approaches are always higher than their respective integral ones. Moreover, at $t = t_4$, the NLSB and ENLG models provide the same damage profile. For $t \geq t_5$, the ENLG model overcomes the NLSB model and becomes the non-local model with the highest damage level until localization, which probably explains that it diffuses damage more than the NLSB and ENLI formulations. Furthermore, one should notice that different models will normally evolve differently during damage growth. However, what remains important is the final representation of the localization phenomenon, as no viscous effect is considered for these approaches. At $t = T$, one may notice that neither the GNL nor the INL formulations reach damage localization for $\alpha = 1.1$. The ENLG model spreads damage over a larger zone compared to the NLSB and ENLI formulations, but still with a damage profile

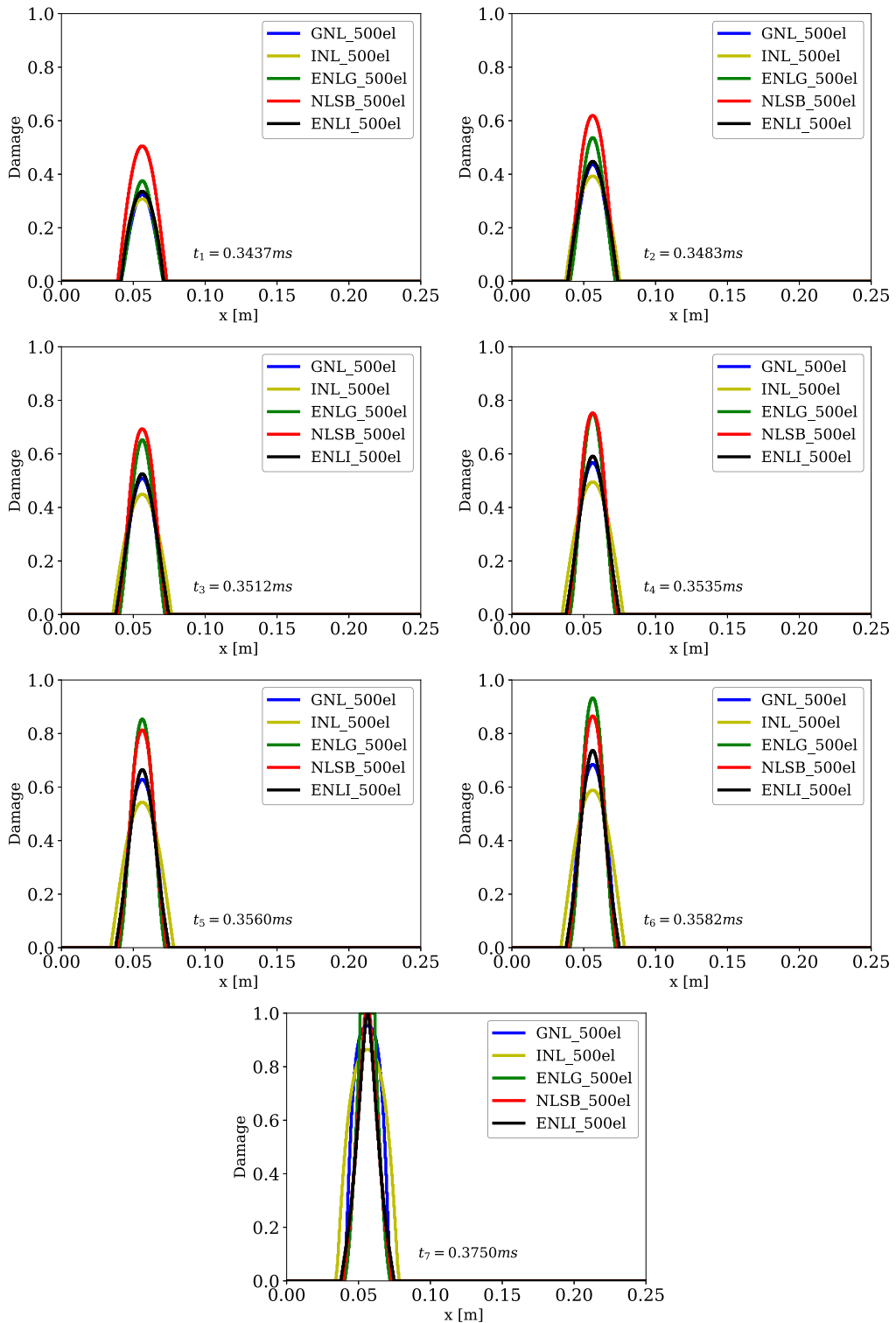


Figure 21. INL, GNL, NLSB, ENLI, and ENLG damage models—damage profiles through time.

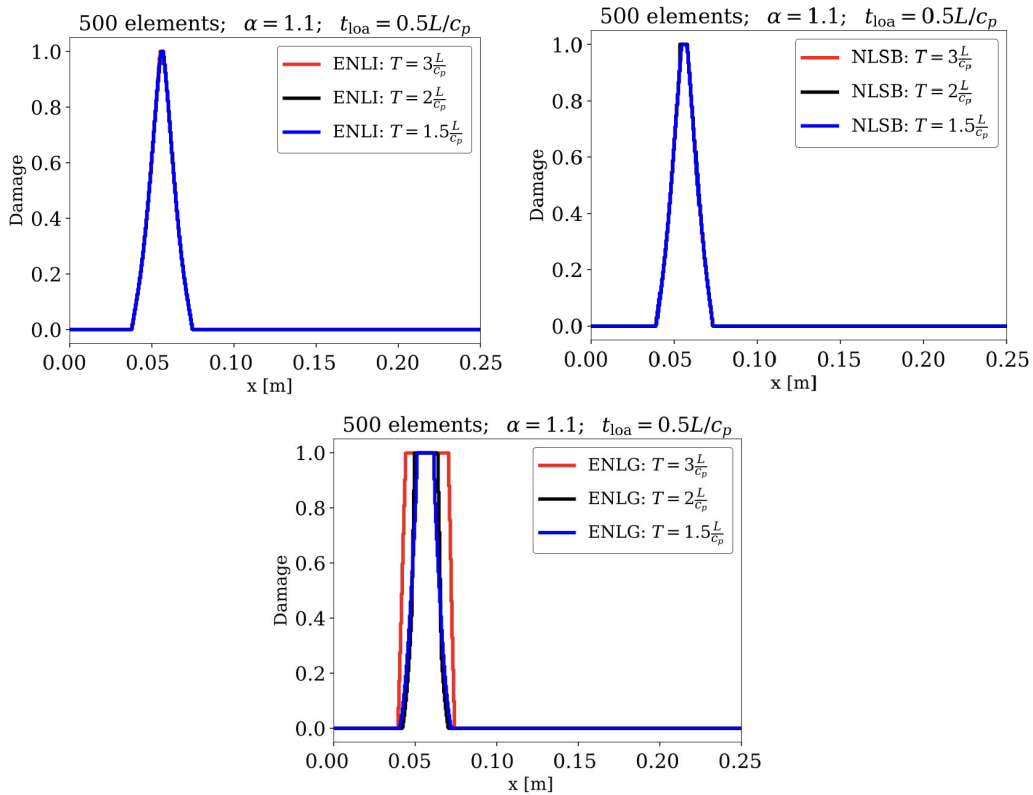


Figure 22. ENLI (top left), NLSB (top right) and ENLG (bottom middle) damage models—damage evolution.

characteristic of evolving non-local models.⁹ Damage evolves faster with the ENLG formulation compared to the other models with evolving distances, but damage diffusion takes place right after localization (see also Figures 18 and 19).

Influence of damage thresholding in the constitutive model numerical integration. Given these results, one may want to limit damage evolution to some smaller critical value for the ENLG model. When applying this procedure only at the behavior law level (i.e., if $D \geq D^*$ then $D = D^*$), the damage profiles computed with the ENLG model show the same behavior as the classic models: damage diffusion and propagation of the damage front when time passes (Figure 22). The ENLG model continues to compute a significant non-local strain field and damage evolves around the localization zone. This does not correspond to the expected theoretical model behavior when non-local interactions through highly damaged zones vanish.

For the ENLI model, the damage profile remains approximately the same (Figure 22 (top left)), with damage starting to localize in three FEs and growing up to four FEs at time $T = 3L/c_p$. In the

⁹These observations make clear that the different non-local models lead to different damage growth rates. Thus, it is expected that the loading parameter α may change the responses. For instance, increasing α implies that damage will attain faster the unity, as seen for the classic models which, for the same plotting time, reach $D = 1$ for $\alpha = 1.5$ but not for $\alpha = 1.1$. On the one hand, such a rapid damage evolution implies that non-locality is more constrained to interact in smaller regions, which can also reduce boundary effects, for example (e.g., Figures 9 and 10 for the ENLG and ENLI models). On the other hand, damage is spread over more elements upon localization.

case of the NLSB model (Figure 22 (top right)), the localization zone increases from seven to eight FEs. In contrast, for the ENLG model (Figure 22 (bottom)), this effect becomes more important as damage is equal to unity in twenty-one FEs for $T = 1.5L/c_p$ up to fifty-two for $T = 3L/c_p$.

It should be noticed that, from a theoretical viewpoint, eikonal formulations (ENLI or ENLG) should not continue to compute a damage evolution after localization [37, 38, 47]. For the ENLI model, the computed effective interaction distances tend to infinity when damage tends to one. Consequently, non-local interactions vanish. The equivalent conclusion for the ENLG model is that the contributions of a highly damaged element in (13) also tend to infinity. Thus, one should expect that after damage localization, the non-local strain field computed by the ENLG model should not evolve in the vicinity of the localized element.¹⁰ In other words, the non-local averaging and the equilibrium equations become uncoupled upon localization, which is the theoretical case for the ENLG model (from a physical viewpoint, micro-cracks should not interact through the new boundary created by a highly damaged zone). However, damage diffusion is much more present in the ENLG formulation, as interactions are directly computed from the FE solving of the Helmholtz-like problem. A similar behavior was described in [30] for a strain-based GNL model without the introduction of artificial modifications to decouple the equilibrium and Helmholtz equations. For ENLI, the computed distances are introduced into the weight function; therefore, the use of an integral approach is more suitable to reduce the interactions numerically.

4.3.4. Numerically modified ENLG

To obtain a numerical approximation of the ENLG model corresponding to its theoretical assumptions, the gradient problem is restated in a modified way. Following the same arguments of Geers *et al.* [30], one can decouple the non-local averaging Helmholtz-type equation from the equilibrium equation when damage tends to unity on a FE. In other words, the non-local equivalent strain is frozen in the localized FE, and interactions between FEs crossed by the damaged band vanish.

From a numerical viewpoint, when damage reaches the limit value $D_c = D^*$ at a given integration point, the second term of the left-hand-side and the right-hand-side in (13) are multiplied by a very large value,¹¹ and the first term of the left-hand-side is multiplied by a null one. This corresponds to the case where damage tends to unity. Such a modification is done at the FE matrix contribution of the localized element and not in the entire domain.

Figure 23 (left) shows the damage profiles obtained with the numerically modified ENLG model for different values of D_c . Plotting time is taken here as $t = T = 1.5L/c_p$. Damage localizes in three FEs for $D_c = 0.99$ (as for the ENLI model, in this case), seven FEs for $D_c = 0.999$ and seventeen for $D_c = 0.9999$. In any case, damage diffusion is drastically reduced compared to the standard ENLG model implementation. Moreover, once the critical condition is attained the damage profile no more evolves (Figure 23 (right)).

Comparison with other formulations: damage diffusion. The comparison between the results given by the ENLI and NLSB models, and the modified ENLG implementation for the loading case A (see Section 4.2) with $\alpha = 1.1$, 500 FEs, and $D_c = D^* = 0.99$ is shown in Figure 24. The damage diffusion issue mentioned previously is solved by applying the modified numerical procedure.

¹⁰Geers *et al.* [30] encountered the same problem when implementing a similar evolving interactions gradient model based on the strain state. The strain-based gradient damage model converged to a discontinuity for high levels of damage ($D = 0.999$). Still, they argued that any further increase in damage at this moment was completely local and of numerical sources. They proposed to stop any evolution of the non-local equivalent strain inside the localized zone when a critical value of the equivalent strain was attained. Moreover, without this modification, they saw oscillations of $\bar{\epsilon}$ in the surroundings of the highly damaged regions, which was responsible for damage evolution in these zones.

¹¹`numpy.inf` in the Python code used in the present work.

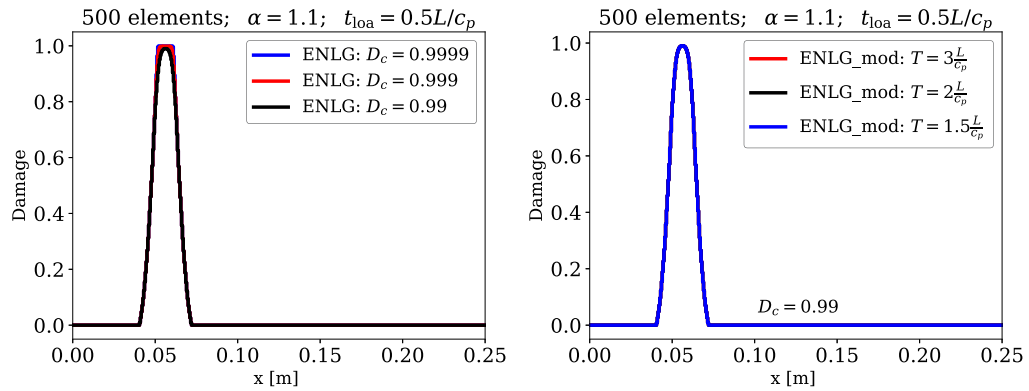


Figure 23. Numerically modified ENLG damage model—damage profiles for different values of D_c (left). Damage profiles evolution for $D_c = 0.99$ (right).

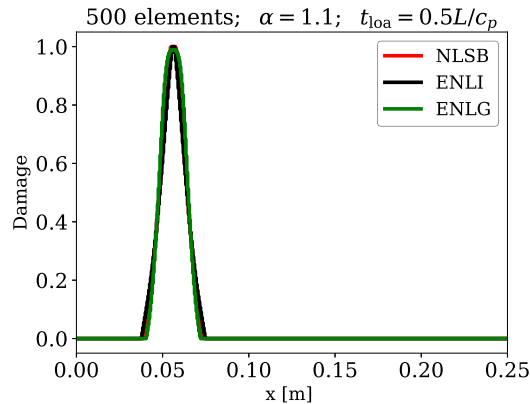


Figure 24. NLSB, ENLI, and numerically modified ENLG damage models. Comparison of damage profiles obtained with $D_c = 0.99$.

The modified ENLG model shows a very similar behavior compared to the NLSB and ENLI formulations, except that it provides a larger damage profile than the other ones for high damage levels.

The corresponding response in terms of the ejection velocity is shown in Figure 25. Once again, $D_c = D^* = 0.99$ for the modified ENLG implementation. Until around 0.4 ms, the ENLG and ENLI models give similar free-face velocity profiles but differ after this point. The NLSB and ENLI formulations give very similar results until the first reflection of the spall signal on the free edge. Despite good localization properties for the modified ENLG with $D_c = 0.99$, the second reflection observed on the free edge is smaller in amplitude than the first one (this does not occur for the standard ENLG, see Figure 25). So, even though the modification works well regarding vanishing non-local interactions, the critical value $D_c = 0.99$ is not large enough to induce almost zero stress upon damage localization. Therefore, the new boundary created by the highly damaged zone is not “perfect” since the stress in damaged zone is still non-zero. Consequently, the free velocity shows a sort of “damping” effect, decreasing the free-edge velocity amplitude after each reflection.

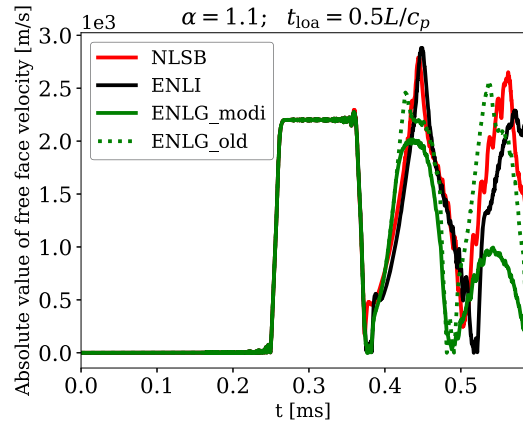


Figure 25. NLSB, ENLI, ENLG, and numerically modified ENLG damage models. Free-surface velocity for a mesh with 500 FEs (loading case A with $\alpha = 1.1$).

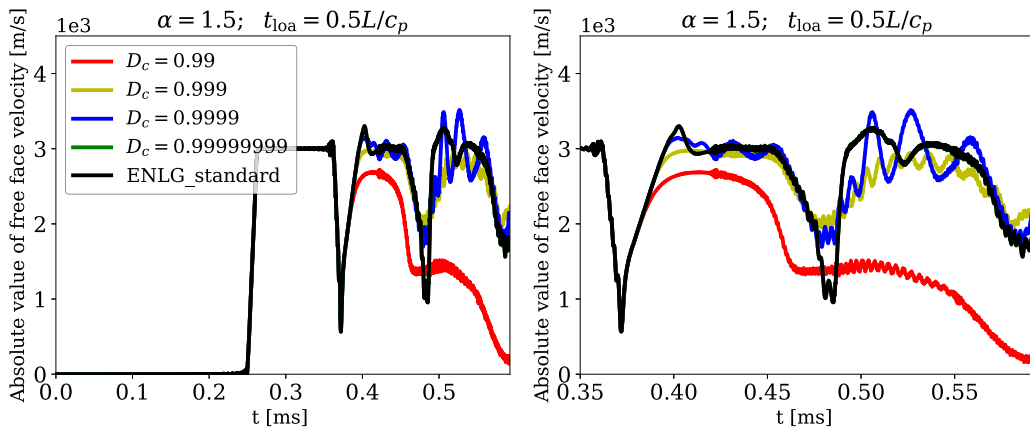


Figure 26. Numerically modified ENLG damage model—free-surface velocities for different values of D_c (loading case A with $\alpha = 1.5$).

This can be further highlighted by analyzing the free-face velocity evolution (the same conditions as in Section 4.3.1 are considered). Figure 26 shows the free-face velocities obtained for the modified ENLG formulation with different values of D_c . One observes the same reducing effects in the velocity amplitude for $D_c = 0.99$, as the state of almost zero stress is not reached. More physical reflections are obtained for higher critical damage values. From $D_c = 0.999$, one may retrieve the behavior of an equivalent of a crack plane working as a newly formed boundary, reflecting the incoming waves. This is in agreement with the damage value found by Geers *et al.* [30] for the completion of localization.

Comparison with other formulations: boundary effect. The modified ENLG approach was also applied to loading case B (see Section 4.2) to analyze its behavior near the free boundary. Damage profiles are given for $t = T = 1.5L/c_p$ for the ENLG model and its modified implementation. As shown in Figure 27 damage attraction to the boundary is not modified by the proposed modification. At the same time, damage diffusion in the middle of the damaged band is strongly reduced: the modified ENLG model localizes damage in only one FE for $\alpha = 1.2$, on three FEs for

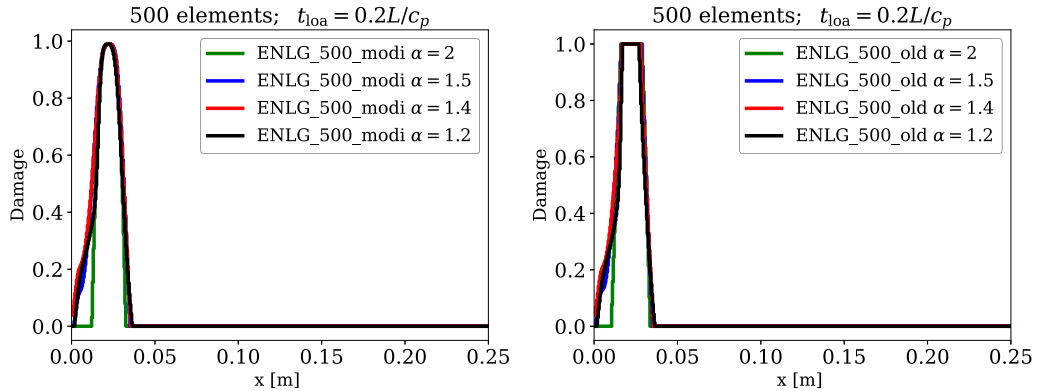


Figure 27. ENLG and numerically modified ENLG damage models—damage profile near the free boundary (loading case B considering different values of α).

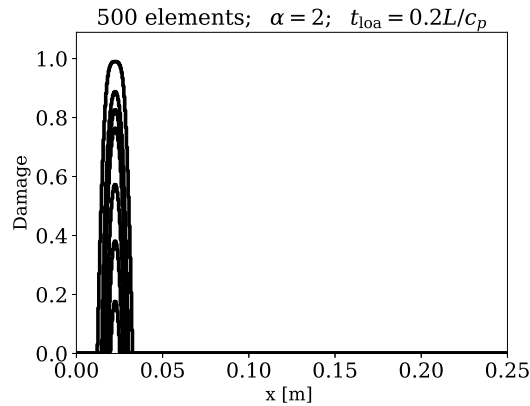


Figure 28. Numerically modified ENLG damage model—damage evolution through time computed with $D_c = 0.99$ near the boundary.

$\alpha = 1.4$, and on four FEs for $\alpha = 1.5$ and $\alpha = 2$. Damage diffusion is significantly bigger with the standard ENLG implementation.

It should be noticed that, once again, a strain rate effect (due to the choice of α) is observed. Choosing $\alpha = 2$ such that there is no damage attraction at all, Figure 28 shows the damage evolution for the modified ENLG model near the boundary. These damage profiles can be directly compared with those obtained with the INL model (see Figure 5 (right)). In that case, damage attraction from the boundary and damage diffusion were observed.

5. Conclusion

A brief review of non-local damage models has been presented. Despite their prominent role in regularizing the structural response when using softening material models, classical non-local approaches with fixed non-local interactions are prone to drawbacks such as damage diffusion across damage bands and damage attraction from the free boundaries. This motivated several authors to propose non-local formulations where non-local interactions evolve with the mechanical fields (damage, stress).

Several non-local damage models were implemented in a FE context, either in integral or gradient form, to highlight the advantages and drawbacks of each approach. Details of each

formulation have been provided. Moreover, a 1D variational formulation has been developed for the ENLG model, entirely based on the one proposed for the classical GNL approach. The so-called spalling problem has been simulated numerically using an *ad-hoc* developed explicit dynamics 1D FE analysis code.

The models have been tested in both damage diffusion and boundary effects situations. The formulations with evolving interactions proved to be more efficient in dealing with the usual problems of classical non-local models. Concerning damage diffusion far from physical boundaries, the eikonal approach has been shown to be more efficient in simulating the bridge between CDM and Fracture Mechanics since the damage field naturally tends to localize in only one FE. Concerning damage evolution close to the boundaries (i.e., the so-called boundary effect), the NLSB model has shown a good response when boundary effects occur, especially when the damaged band is located close to the free edge. The eikonal formulations are more sensitive to boundary effects. The ENLG model is less affected by the free boundary problem when compared to the ENLI formulation. The ENLG model shows, however, an unexpected damage diffusion upon localization. This latter spurious response was treated by a numerical procedure limiting damage to a critical value (modified ENLG), similar to the one proposed in [30]. The modified ENLG model has shown good localization properties and satisfactory behavior near the boundary. However, loading parameters may have an important influence on damage diffusion and boundary effects. Consequently, the strain rate should not be neglected if one aims to model the real behavior of a given material. In any case, non-local models with evolving interactions have proved more efficient than the classical ones in estimating the spall location.

A proper non-local formulation should not only behave well in the case of existing boundaries but also in the case where macro-cracks (highly damaged zones in a CDM context) are formed, and new boundaries are created. In these situations, non-local interactions should evolve so that the response becomes local.

Concerning the behavior close to existing boundaries, the NLSB model provided satisfactory results as the stress state is considered in the averaging procedure. The eikonal models are more adapted to treat a newly created boundary, as the interaction distance between a highly damaged element and its neighbors naturally tends to infinity, and non-local interactions are stopped. This is confirmed by the free-surface velocity profiles, where the spall signal shows wave reflections on this newly created boundary.

A mathematical analysis of the localizing properties of evolving interactions' non-local models should be carried out to confirm the results summarized earlier. This may also be extended to more complex cases, such as anisotropic damage. A non-local damage model considering evolving interactions should be capable of dealing with existing boundaries and newly-formed ones by highly damaged zones. One proper way to model this would be to consider a modified Riemannian metric inside the derivation of the eikonal approach, taking into account both the damage and stress field, for instance.

Finally, it should be noticed that close to failure, the strong localization of the mechanical fields cannot be reproduced in a relevant way in a standard FE formulation supposing the continuity of the displacement field. Right after localization, the transition from a regularized continuum model to an explicit crack description should be applied [60–64]. In the case of spalling, for instance, a complete simulation of failure would couple damage to a strong discontinuity, ejecting some part of the specimen and physically dividing it in two separate domains.

Conflicts of interest

The authors declare that they have no known competing financial interests or personal relationships that could have appeared to influence the work reported in this paper.

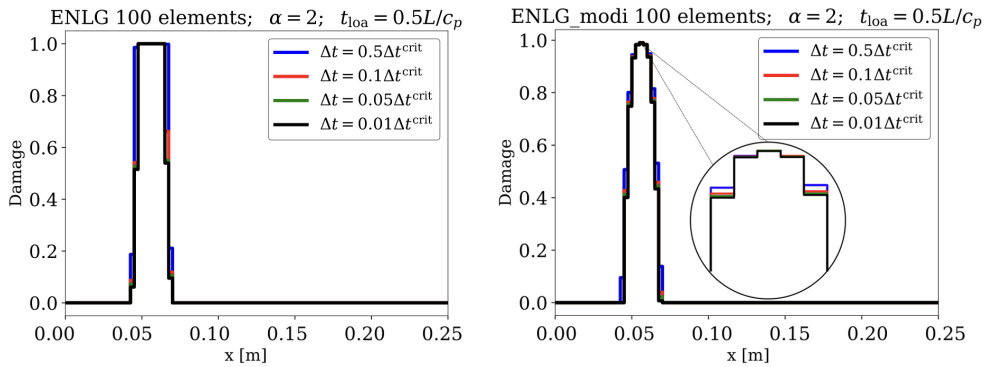


Figure 29. ENLG (left) and numerically modified ENLG (right) damage models—convergence upon time step refinement in damage profiles considering $D_c = 0.99$.

Dedication

The manuscript was written through contributions of all authors. All authors have given approval to the final version of the manuscript.

Acknowledgments

This work is supported by a public grant overseen by the French National research Agency (ANR) as part of the « Investissements d’Avenir » program, through the “ADI 2021” project funded by the IDEX Paris-Saclay, ANR-11-IDEX-0003-02. The University of Molise, Italy, is also acknowledged for its financial support. G. Rastello was supported by the SEISM Institute, France (<http://www.institut-seism.fr>).

Appendix A. Influence of the time step on the damaging process

As it is well known, the explicit time-integration scheme employed in this work allows limiting calculation timings (there is no need to invert the stiffness matrix) but is conditionally stable. For all the results provided in this work, the time step was set to $\Delta t = \Delta t^{\text{crit}}/2$ to guarantee stable results. A few additional results are illustrated in the following to demonstrate that the damage diffusion and boundary effects observed converge upon time refinement.

As shown in Figures 29–31, concerning the ENLI and ENLG (standard and numerically modified versions) models, further reductions of the time step (i.e., $\Delta t < \Delta t^{\text{crit}}/2$) do not lead to different results. Same considerations can be made for the NLSB formulation.

As illustrated in Figures 9 and 11, secondary damaged areas may appear when considering damage close to the boundary. In that case, further time step reductions do not strongly affect the damage profiles (Figure 32). For instance, two secondary damaged zones are obtained for $\alpha = 2$ and only one for $\alpha = 1.5$. For $\alpha = 1.4$, no secondary damaged zones are observed. The appearance of such minor damaged regions is not a consequence of the various reflected waves after the main damage band localization, as they appear almost at the same moment as the main damaged region. Instead, their appearance is directly related to some oscillations (Figure 33 (right)) in the stress field that is directly considered for computing non-local interactions. Moreover, the higher the α higher the amplitude of these oscillations. To alleviate this effect, a low-pass filter may be applied to the stress field (the results presented in this work are obtained without filtering the

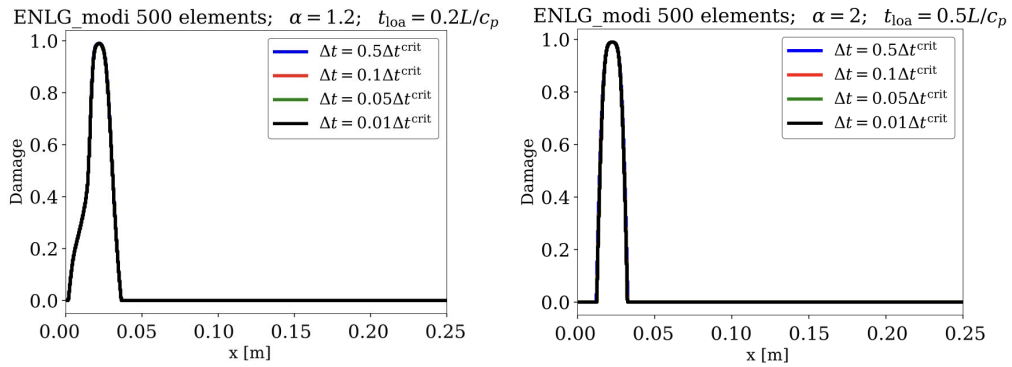


Figure 30. Numerically modified ENLG damage model—convergence upon time step refinement in damage profiles considering $D_c = 0.99$. Loading case B with $\alpha = 1.2$ (left) and $\alpha = 2$ (right).

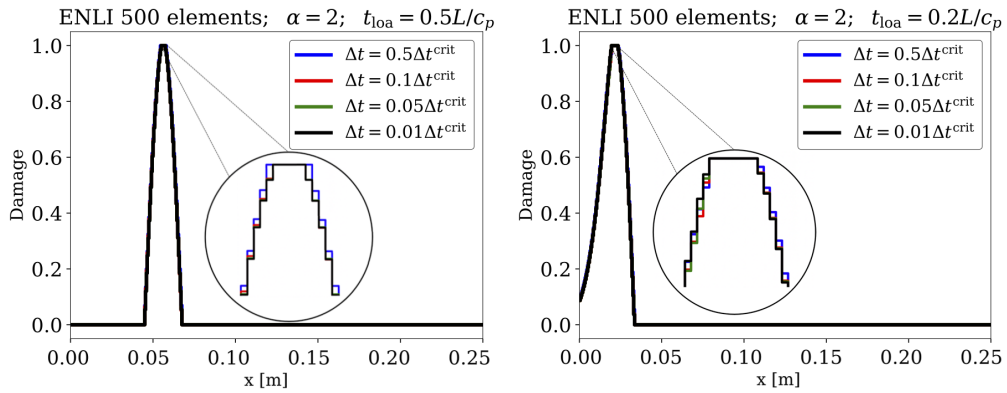


Figure 31. ENLI damage model—convergence upon time step refinement in damage profiles. Loading case A (left) and loading case B (right).

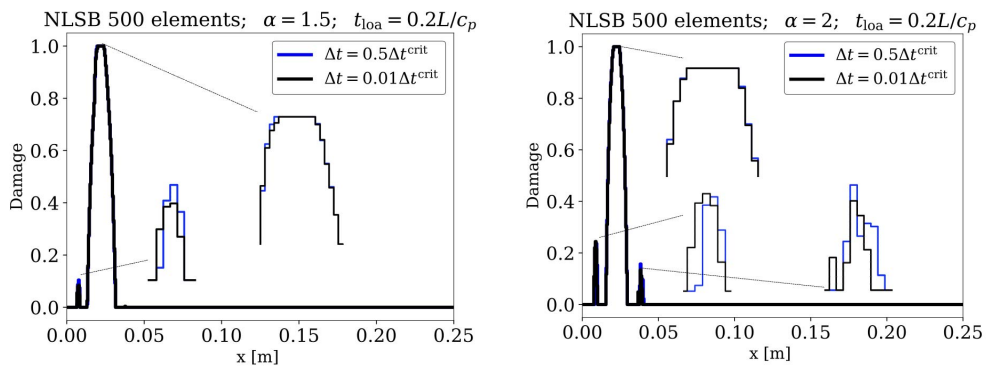


Figure 32. NLSB damage model—convergence upon time step refinement in the damage profile considering the loading case B.

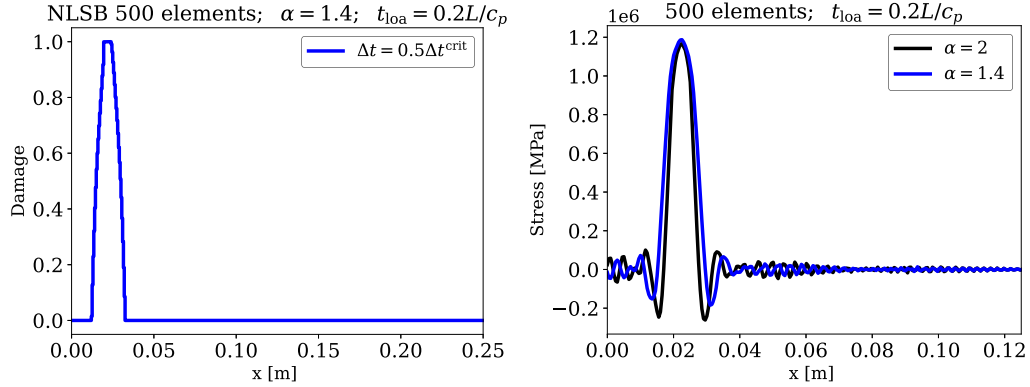


Figure 33. NLSB damage model—damage profile computed for the loading case B with $\alpha = 1.4$ (left). Stress field along the bar for $\alpha = 1.4$ and $\alpha = 2$ (right).

stress). Oscillations in the non-local equivalent strain field in the gradient version of NLSB were already reported in [39].

In conclusion, these results prove that convergence regarding time step refinement is obtained. As a consequence, the results given for $\Delta t = 0.5\Delta t^{\text{crit}}$ are already sufficient to provide representative results of the models' behavior.

Appendix B. Semi-analytical comparative study for the integral models

To further compare the INL, ENLI and NLSB models in the computation of the non-local equivalent strain field, a semi-analytical study is developed.¹² Figure 34 illustrates the problem considered. It is assumed that a monotonic response leads to a given mechanical state in the bar. At time t_n , the mechanical state of the bar is described by $\varepsilon(x, t) = \varepsilon_1[\mathcal{H}(x - \ell) - \mathcal{H}(x - \ell - h)]$, $D(x, t) = D_1[\mathcal{H}(x - \ell) - \mathcal{H}(x - \ell - h)]$, and $\sigma(x, t) = E(1 - D_1)\varepsilon_1[\mathcal{H}(x - \ell) - \mathcal{H}(x - \ell - h)]$. Here, ℓ is the distance between the damaged FE and the left boundary. Moreover ε_1 , D_1 and σ_1 are respectively the strain, the damage and the stress amplitude in the damaged FE at time t_n ; $\mathcal{H}(x) = 1$ if $x \geq 0$, $\mathcal{H}(x) = 0$ otherwise, is the Heaviside function. To compare the different formulations, a strain increment is applied to the bar at time t_{n+1} :

$$\Delta\varepsilon(x, t) = \Delta\varepsilon^*[\mathcal{H}(x - \ell) - \mathcal{H}(x - \ell - h)] \quad (23)$$

and the resulting non-local equivalent strain and damage fields are computed.

B.1. Non-local strain fields

Let us consider the same FE discretization of the bar as in Section 3.1. The analytical expressions of the non-local equivalent strain field given by each model (at integration point x_i) are approximated by numerical integration as (in the following, $x^* = \ell + h/2$):

- INL.

$$\bar{\varepsilon}_{\text{INL}}(x_i, t + \Delta t) = (\varepsilon_1 + \Delta\varepsilon^*) \frac{\exp\left(-4\frac{(x_i - x^*)^2}{\ell_c^2}\right)}{\sum_j \exp\left(-4\frac{(x_i - x_j)^2}{\ell_c^2}\right)} \quad (24)$$

¹²A similar comparison involving the implicit gradient formulations (GNL and ENLG) is left for future work.

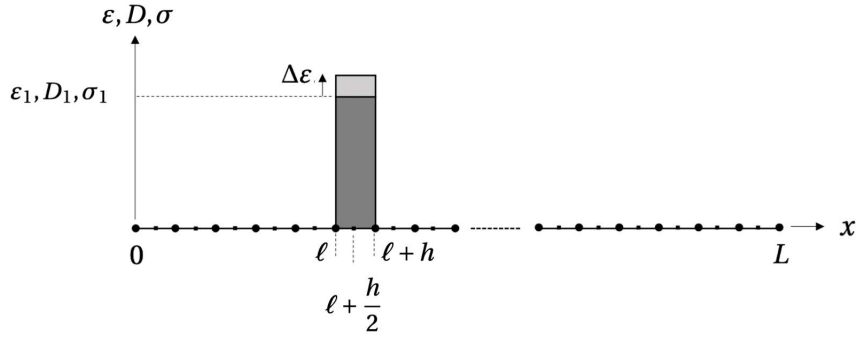


Figure 34. Semi-analytical study—schematic representation of the strain, damage and stress fields along the bar.

- NLSB.

$$\bar{e}_{\text{NLSB}}(x_i, t + \Delta t) = (\varepsilon_1 + \Delta\varepsilon^*) \frac{\exp\left(-4 \frac{(x_i - x^*)^2}{\left(\frac{\sigma_1}{f_t} \ell_c\right)^2}\right)}{1 + \exp\left(-4 \frac{(x_i - x^*)^2}{\left(\frac{\sigma_1}{f_t} \ell_c\right)^2}\right)} \quad \forall x_i \neq x^* \quad (25)$$

$$\bar{e}_{\text{NLSB}}(x_i, t + \Delta t) = (\varepsilon_1 + \Delta\varepsilon^*) \quad x_i = x^* \quad (26)$$

- ENLI.

$$\bar{e}_{\text{ENLI}}(x_i, t + \Delta t) = (\varepsilon_1 + \Delta\varepsilon^*) \frac{\exp\left(-4 \frac{\left(|x_i - x^*| + \frac{h}{2} \left(\frac{1}{\sqrt{1-D_1}} - 1\right)\right)^2}{\ell_c^2}\right)}{V_r(x)} \quad \forall x_i \neq x^* \quad (27)$$

$$\bar{e}_{\text{ENLI}}(x_i, t + \Delta t) = (\varepsilon_1 + \Delta\varepsilon^*) \frac{1}{1 + \sum_j \exp\left(-4 \frac{\left(|x^* - x_j| + \frac{h}{2} \left(\frac{1}{\sqrt{1-D_1}} - 1\right)\right)^2}{\ell_c^2}\right)} \quad x_i = x^* \quad (28)$$

with:

$$V_r^1(x_i) = \sum_j \mathcal{H}[(x_j - x^*)(x_i - x^*)] \exp\left(-4 \frac{(x_i - x_j)^2}{\ell_c^2}\right) \quad (29)$$

$$V_r^2(x_i) = \sum_k \mathcal{H}[-(x_k - x^*)(x_i - x^*)] \exp\left(-4 \frac{\left(|x_i - x_k| + h \left(\frac{1}{\sqrt{1-D_1}} - 1\right)\right)^2}{\ell_c^2}\right) \quad (30)$$

$$V_r^3(x_i) = \exp\left(-4 \frac{\left(|x_i - x^*| + \frac{h}{2} \left(\frac{1}{\sqrt{1-D_1}} - 1\right)\right)^2}{\ell_c^2}\right) \quad (31)$$

$$V_r(x_i) = V_r^1(x_i) + V_r^2(x_i) + V_r^3(x_i) \quad (32)$$

B.2. Results

A FE mesh with 100 elements is considered. Material parameters are the same as that used in the rest of the work. Once again, two situations are studied: damaging far from the boundary and damaging close to the boundary.

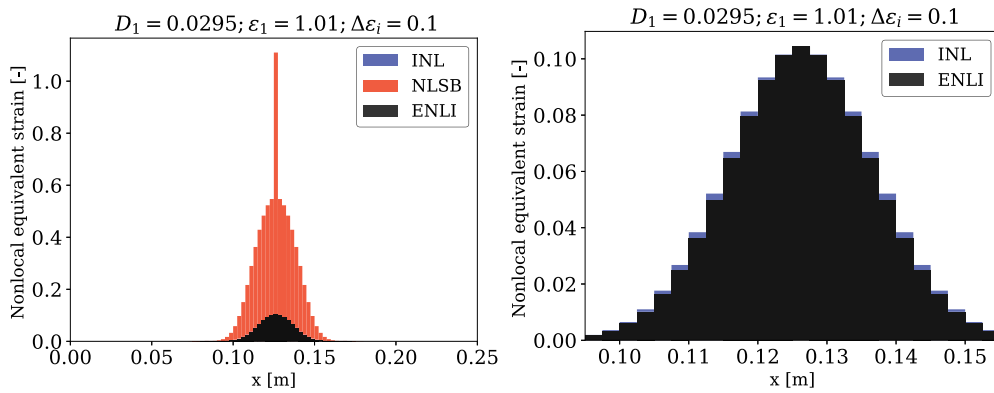


Figure 35. Semi-analytical study—non-local equivalent strain field for the three integral models studied at a low damage level D_1 .

B.3. Damage far from the boundary

Let us first consider a damaged element located in the middle of the bar. In this example, $\varepsilon_1 = 1.01$ indicates that the material is already damaged (i.e., $\varepsilon_1 > \kappa_0$) with D_1 computed by its evolution law. As developed before, the non-local equivalent strain will always be equal to the local one for the NLSB model, in the FE where the strain is considered to evolve (Figure 35). Four cases can be distinguished:

- (i) *Very low damage level.* The ENLI and INL models give almost identical non-local equivalent strain profiles (Figure 35 (right)).
- (ii) *Moderate damage level.* The NLSB model presents a thinner non-local equivalent strain profile, which is a consequence of the modified interactions due to the reductions in the stress field (Figure 36). The ENLI and INL models give similar results but slightly differ at the central FE where \bar{e} is bigger for the ENLI model.
- (iii) *High damage level.* The non-local equivalent strain field is almost fully concentrated in the central FE for the NLSB model, where one has always $\bar{e} = e$ (Figure 37). As a consequence of strain localization, the values of \bar{e} in the neighboring elements are very low, which means that non-local interactions are vanishing. The differences between the profiles of \bar{e} for the ENLI and INL models can be clearly observed in Figure 37 (right). The ENLI model shows a thinner non-local strain profile, and the non-local equivalent strain is concentrated in the central FE but not yet equal to the local one.
- (iv) *Damage close to one.* Let us finally consider the case of $D_1 = 1$. In this situation, the ENLI model shows a profile where $\bar{e} = e$ in the central FE, and there is no other non-local equivalent strain in the bar (Figure 38 (left)). Strain localizes, and interactions naturally vanish. For the central FE, the NLSB and ENLI models give similar results when damage attains unity. However, there is still some \bar{e} computed in the vicinity of the localized element for the NLSB model (Figure 38 (right)).

In conclusion, the fact that \bar{e} is always equal to e in the central FE makes damage evolve faster for the NLSB model than the other models. Moreover, as expected, the state of the material at a given time does not influence the form of the non-local equivalent profile for the INL model. Until a moderate damage level, the ENLI and INL models should thus give similar damage growths. Finally, the ENLI model naturally recovers locality when the damage is large enough (i.e., a new boundary is formed and interactions vanish entirely).

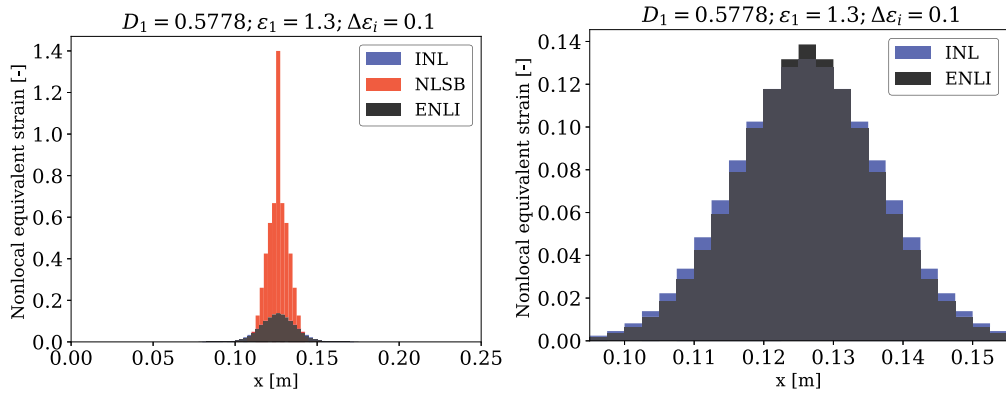


Figure 36. Semi-analytical study—non-local equivalent strain field for the three integral models studied at a moderate damage level D_1 .

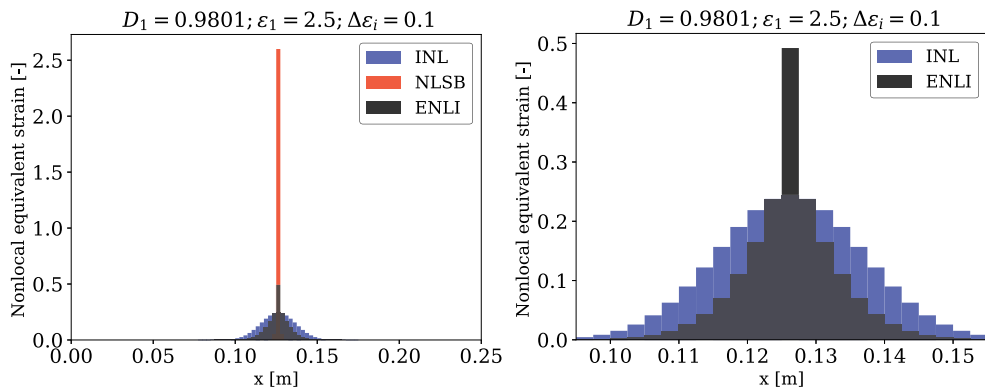


Figure 37. Semi-analytical study—non-local equivalent strain field for the three integral models studied at an high damage level D_1 .

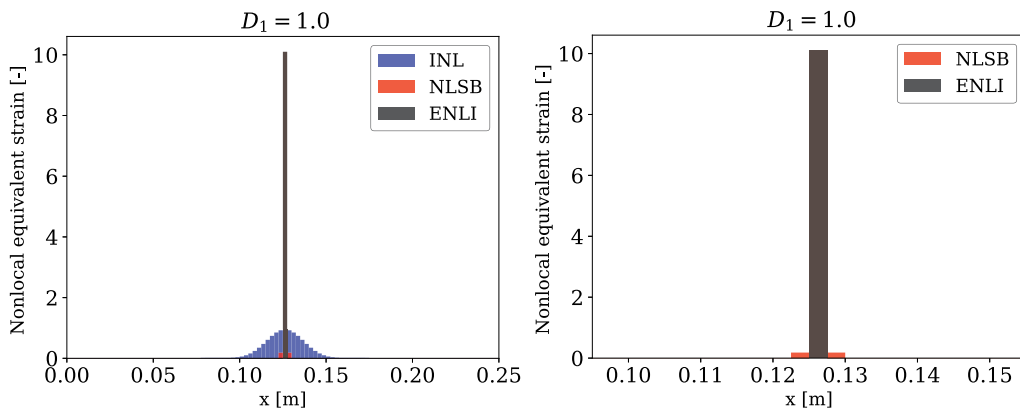


Figure 38. Semi-analytical study—non-local equivalent strain field for the three integral models studied at $D_1 = 1$.

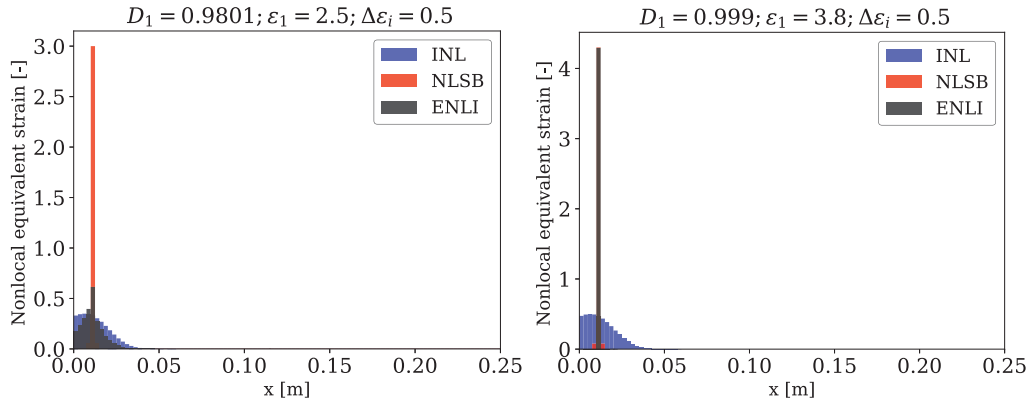


Figure 39. Semi-analytical study—non-local equivalent strain field for the three integral models studied at an high damage level D_1 (left) and $D_1 = 0.999$ (right) when near the boundary.

B.4. *Damage near the boundary*

Figure 39 compares the three integral models when computing a non-local field given a mechanical state in a FE near the boundary. The non-local equivalent strain calculated by the INL model is attracted by the boundary, which corresponds to the results presented in [27]. The damage profile for this model will then gradually evolve and shift to the free edge during spalling formation.

For a high damage level, the non-local equivalent strain computed by the ENLI model still presents some minor attraction to the boundary compared to the INL model. The maximum of \bar{e} takes place in the FE where strain is increasing and is more significant than in the neighboring elements. This kind of behavior, in terms of damage profile, was also illustrated in Figures 9 and 10 based on numerical results. During damage evolution, some attraction will take place for the ENLI model. Still, upon damage localization, this effect vanishes in the localized zone. As a consequence, the maximum damage does not shift to the free edge (i.e., the ENLI model retrieves a local behavior with no attraction at all). Minor boundary effects will inevitably happen for this model, but damage-dependent vanishing interactions will prevent the shift of maximum damage to the free edge.¹³

The NLSB model naturally considers geometrical boundaries in its formulation, as interactions depend on the stress state. Figure 39 shows the non-local equivalent strain field computed for this model. Differently from the INL and ENLI models, the field \bar{e} shows no attraction to the free edge. Moreover, the maximum of \bar{e} is attained where damage occurs since $\bar{e} = e$ in the FE where strain is increased.

References

- [1] G. Pijaudier-Cabot, Z. P. Bažant, “Nonlocal damage theory”, *J. Eng. Mech.* **113** (1987), no. 10, p. 1512-1533.
- [2] A. Benallal, R. Billardon, G. Geymonat, “Bifurcation and localization in rate-independent materials. Some general considerations”, in *Bifurcation and Stability of Dissipative Systems*, Springer, Vienna, 1993, p. 1-44.

¹³Since this model considers only the damage state variable to modify the interactions, one way to avoid these effects is to introduce virtual materials completely damaged (i.e., $D = 1$) on the boundaries. This would lead to an additional computational cost and the need of pre-processing techniques. We recall that the eikonal approach was derived for an infinite body. Therefore, the ENLI model naturally takes into account the so-called evolving boundaries effects introduced by newly formed damaged zones. However, existing boundaries were not considered in the development of this approach.

- [3] H. Read, G. Hegemier, "Strain softening of rock, soil and concrete—A review article", *Mech. Mater.* **3** (1984), no. 4, p. 271-294.
- [4] E. Rizzi, I. Carol, K. Willam, "Localization analysis of elastic degradation with application to scalar damage", *J. Eng. Mech.* **121** (1995), no. 4, p. 541-554.
- [5] R. H. J. Peerlings, "Enhanced damage modelling for fracture and fatigue", PhD Thesis, Technische Universiteit Eindhoven, 1999.
- [6] A. Hillerborg, M. Modeer, P. Petersson, "Analysis of crack formation and crack growth in concrete by means of fracture mechanics and finite elements", *Cem. Concr. Res.* **6** (1976), no. 6, p. 773-781.
- [7] J. Mosler, G. Meschke, "Embedded crack vs. smeared crack models: a comparison of elementwise discontinuous crack path approaches with emphasis on mesh bias", *Comput. Methods Appl. Mech. Eng.* **193** (2004), no. 30–32, p. 3351-3375.
- [8] M. Jirásek, P. Grassl, "Evaluation of directional mesh bias in concrete fracture simulations using continuum damage models", *Eng. Fract. Mech.* **75** (2008), no. 8, p. 1921-1943.
- [9] Z. P. Bažant, "Why continuum damage is nonlocal: justification by quasiperiodic microcrack array", *Mech. Res. Commun.* **14** (1987), no. 5–6, p. 407-419.
- [10] Z. P. Bažant, M. Jirásek, "Nonlocal integral formulations of plasticity and damage: survey of progress", *J. Eng. Mech.* **128** (2002), no. 11, p. 1119-1149.
- [11] E. C. Aifantis, "On the microstructural origin of certain inelastic models", *J. Eng. Mater. Technol.* **106** (1984), no. 4, p. 326-330.
- [12] D. Lasry, T. Belytschko, "Localization limiters in transient problems", *Int. J. Solids Struct.* **24** (1988), no. 6, p. 581-597.
- [13] E. C. Aifantis, "The physics of plastic deformation", *Int. J. Plast.* **3** (1987), no. 3, p. 211-247.
- [14] H. B. Mühlhaus, E. C. Aifantis, "A variational principle for gradient plasticity", *Int. J. Solids Struct.* **28** (1991), p. 845-857.
- [15] B. Nedjar, "Mécanique de l'endommagement. Théorie du premier gradient et application au béton", PhD Thesis, Ecole Nationale des Ponts et Chaussées, 1995.
- [16] R. Peerlings, R. de Borst, W. Brekelmans, J. de Vree, "Gradient-enhanced damage model for quasi-brittle materials", *Int. J. Numer. Methods Eng.* **39** (1996), p. 391-403.
- [17] O. Allix, J. Deü, "Delay-damage modelling for fracture prediction of laminated composites under dynamic loading", *Eng. Trans.* **45** (1997), no. 1, p. 29-46.
- [18] O. Allix, P. Feissel, P. Thévenet, "A delay damage mesomodel of laminates under dynamic loading: basic aspects and identification issues", *Comput. Struct.* **81** (2003), no. 12, p. 1177-1191.
- [19] R. Desmorat, M. Chambart, F. Gatuingt, D. Guilbaud, "Delay-active damage versus non-local enhancement for anisotropic damage dynamics computations with alternated loading", *Eng. Fract. Mech.* **77** (2010), no. 12, p. 2294-2315.
- [20] N. Moës, C. Stolz, P.-E. Bernard, N. Chevaugeon, "A level set based model for damage growth: the thick level set approach", *Int. J. Numer. Methods Eng.* **86** (2011), no. 3, p. 358-380.
- [21] G. Francfort, J.-J. Marigo, "Revisiting brittle fracture as an energy minimization problem", *J. Mech. Phys. Solids* **46** (1998), no. 8, p. 1319-1342.
- [22] B. Bourdin, G. Francfort, J.-J. Marigo, "Numerical experiments in revisited brittle fracture", *J. Mech. Phys. Solids* **48** (2000), no. 4, p. 797-826.
- [23] N. Moës, N. Chevaugeon, "Lipschitz regularization for softening material models: the Lip-field approach", *C. R. Mécanique* **349** (2021), no. 2, p. 415-434.
- [24] J. Klepaczko, A. Brara, "An experimental method for dynamic tensile testing of concrete by spalling", *Int. J. Impact Eng.* **25** (2001), p. 387-409.
- [25] H. Schuler, C. Mayrhofer, K. Thoma, "Spall experiments for the measurement of the tensile strength and fracture energy of concrete at high strain rates", *Int. J. Impact Eng.* **32** (2006), no. 10, p. 1635-1650.
- [26] B. Erzar, P. Forquin, "An experimental method to determine the tensile strength of concrete at high rates of strain", *Exp. Mech.* **50** (2010), no. 7, p. 941-955.
- [27] A. Krayani, G. Pijaudier-Cabot, F. Dufour, "Boundary effect on weight function in nonlocal damage model", *Eng. Fract. Mech.* **76** (2009), no. 14, p. 2217-2231.
- [28] A. Simone, H. Askes, L. J. Sluys, "Incorrect initiation and propagation of failure in non-local and gradient-enhanced media", *Int. J. Solids Struct.* **41** (2004), no. 2, p. 351-363.
- [29] Z. P. Bažant, "Why continuum damage is nonlocal: micromechanics arguments", *J. Eng. Mech.* **117** (1991), no. 5, p. 1070-1087.
- [30] M. Geers, R. de Borst, W. Brekelmans, R. Peerlings, "Strain-based transient-gradient damage model for failure analyses", *Comput. Methods Appl. Mech. Eng.* **160** (1998), no. 1–2, p. 133-153.
- [31] C. Giry, F. Dufour, J. Mazars, "Stress-based nonlocal damage model", *Int. J. Solids Struct.* **48** (2011), no. 25–26, p. 3431-3443.

- [32] Z. P. Bažant, “Nonlocal damage theory based on micromechanics of crack interactions”, *J. Eng. Mech.* **120** (1994), p. 593-617.
- [33] G. Pijaudier-Cabot, K. Haidar, J.-F. Dubé, “Non-local damage model with evolving internal length”, *Int. J. Numer. Anal. Methods Geomech.* **28** (2004), no. 78, p. 633-652.
- [34] R. Desmorat, F. Gatuingt, “Introduction of an internal time in nonlocal integral theories”, 2007, Internal Report LMT-Cachan. ENS Cachan/CNRS/Université Paris 6/PRES Unive 268.
- [35] G. Pijaudier-Cabot, F. Dufour, “Non local damage model: boundary and evolving boundary effects”, *Eur. J. Environ. Civ. Eng.* **14** (2010), no. 6–7, p. 729-749.
- [36] G. D. Nguyen, “A damage model with evolving nonlocal interactions”, *Int. J. Solids Struct.* **48** (2011), no. 10, p. 1544-1559.
- [37] R. Desmorat, F. Gatuingt, M. Jirásek, “Nonlocal models with damage-dependent interactions motivated by internal time”, *Eng. Fract. Mech.* **142** (2015), p. 255-275.
- [38] G. Rastello, C. Giry, F. Gatuingt, R. Desmorat, “From diffuse damage to strain localization from an Eikonal Non-Local (ENL) Continuum Damage model with evolving internal length”, *Comput. Methods Appl. Mech. Eng.* **331** (2018), p. 650-674.
- [39] B. Vandoren, A. Simone, “Modeling and simulation of quasi-brittle failure with continuous anisotropic stress-based gradient-enhanced damage models”, *Comput. Methods Appl. Mech. Eng.* **332** (2018), p. 644-685.
- [40] M. Jirásek, R. Desmorat, “Localization analysis of nonlocal models with damage-dependent nonlocal interaction”, *Int. J. Solids Struct.* **174–175** (2019), p. 1-17.
- [41] L. M. Kachanov, “Time of rupture process under creep conditions (in Russian)”, *Izv. Acad. Nauk, USSR* **8** (1958), p. 26-31.
- [42] P. Feenstra, “Computational aspects of biaxial stress in plain reinforced concrete”, PhD Thesis, TU Delft, 1993.
- [43] M. Jirásek, “Nonlocal models for damage and fracture: comparison of approaches”, *Int. J. Solids Struct.* **35** (1998), no. 31–32, p. 4133-4145.
- [44] R. Peerlings, M. Geers, R. de Borst, W. Brekelmans, “A critical comparison of nonlocal and gradient-enhanced softening continua”, *Int. J. Solids Struct.* **38** (2001), no. 44–45, p. 7723-7746.
- [45] R. Peerlings, T. Massart, M. Geers, “A thermodynamically motivated implicit gradient damage framework and its application to brick masonry cracking”, *Comput. Methods Appl. Mech. Eng.* **193** (2004), no. 30–32, p. 3403-3417.
- [46] A. Simone, “Explicit and implicit gradient-enhanced damage models”, *Rev. Eur. Génie Civ.* **11** (2007), no. 7–8, p. 1023-1044.
- [47] F. Thierry, G. Rastello, C. Giry, F. Gatuingt, “One-dimensional Eikonal Non-Local (ENL) damage models: influence of the integration rule for computing interaction distances and indirect loading control on damage localization”, *Mech. Res. Commun.* **110** (2020), article no. 103620.
- [48] G. Pijaudier-Cabot, D. Grégoire, “A review of non local continuum damage: modelling of failure?”, *Netw. Heterog. Media* **9** (2014), no. 4, p. 575-597.
- [49] L. B. Rojas-Solano, D. Grégoire, G. Pijaudier-Cabot, “Interaction-based non-local damage model for failure in quasi-brittle materials”, *Mech. Res. Commun.* **54** (2013), p. 56-62.
- [50] G. Rastello, H. L. Oliveira, A. Millard, “Path-following methods for unstable structural responses induced by strain softening: a critical review”, *C. R. Mécanique* **350** (2022), p. 205-236.
- [51] A. Simone, H. Askes, R. H. J. Peerlings, L. J. Sluys, “Interpolation requirements for implicit gradient-enhanced continuum damage models”, *Commun. Numer. Methods Eng.* **19** (2003), no. 7, p. 563-572.
- [52] E. Azinpour, J. P. S. Ferreira, M. P. L. Parente, J. C. de Sa, “A simple and unified implementation of phase field and gradient damage models”, *Adv. Model. Simul. Eng. Sci.* **5** (2018), no. 1, article no. 15.
- [53] R. de Borst, A. Benallal, O. Heeres, “A gradient-enhanced damage approach to fracture”, *J. Phys. IV France* **6** (1996), no. C6, p. C6-491-C6-502.
- [54] Z. P. Bažant, T. B. Belytschko, “Wave propagation in a strain-softening bar: exact solution”, *J. Eng. Mech.* **111** (1985), no. 3, p. 381-389.
- [55] D. Dandekar, P. Bartkowski, “Tensile strengths of silicon carbide (SiC) under shock loading”, Tech. Report ARL-TR-2430, Army Research Laboratory, Aberdeen Proving Ground, 2001.
- [56] D. Dandekar, “Shock response of boron carbide”, Tech. Report ARL-TR-2456, Army Research Laboratory, Aberdeen Proving Ground, 2001.
- [57] S. Mariani, G. Gobat, “Identification of strength and toughness of quasi-brittle materials from spall tests: a Sigma-point Kalman filter approach”, *Inverse Probl. Sci. Eng.* **27** (2019), no. 9, p. 1318-1346.
- [58] G. Camacho, M. Ortiz, “Computational modelling of impact damage in brittle materials”, *Int. J. Solids Struct.* **33** (1996), no. 20–22, p. 2899-2938.
- [59] S. Forest, “Micromorphic approach for gradient elasticity, viscoplasticity, and damage”, *J. Eng. Mech.* **135** (2009), no. 3, p. 117-131.
- [60] J. Mazars, G. Pijaudier-Cabot, “From damage to fracture mechanics and conversely: a combined approach”, *Int. J. Solids Struct.* **33** (1996), no. 20–22, p. 3327-3342.

- [61] M. Jirasek, T. Zimmermann, "Embedded crack model. Part II: combination with smeared cracks", *Int. J. Numer. Methods Eng.* **50** (2001), no. 6, p. 1291-1305.
- [62] A. Simone, G. N. Wells, L. J. Sluys, "From continuous to discontinuous failure in a gradient-enhanced continuum damage model", *Comput. Methods Appl. Mech. Eng.* **192** (2003), no. 41-42, p. 4581-4607.
- [63] F. Cazes, M. Coret, A. Combescure, A. Gravouil, "A thermodynamic method for the construction of a cohesive law from a nonlocal damage model", *Int. J. Solids Struct.* **46** (2009), no. 6, p. 1476-1490.
- [64] S. Cu villiez, F. Feyel, E. Lorentz, S. Michel-Ponnelle, "A finite element approach coupling a continuous gradient damage model and a cohesive zone model within the framework of quasi-brittle failure", *Comput. Methods Appl. Mech. Eng.* **237-240** (2012), p. 244-259.